UVicSPACE: Research & Learning Repository

University of Victoria

Faculty of Science

Faculty Publications

Calcium carbonate hexahydrate (ikaite): History of mineral formation as recorded by stable isotopes

Whiticar, M. J., Suess, E., Wefer, E., & Müller, P. J.

2022

© 2022 Michael J. Whiticar et al. This is an open access article distributed under the terms of the Creative Commons Attribution License.
http://creativecommons.org/licenses/by/4.0/

This article was originally published at:
https://doi.org/10.3390/min12121627

Citation for this paper:

Whiticar, M. J., Suess, E., Wefer, G., & Müller, P. J. (2022). "Calcium carbonate hexahydrate (ikaite): History of mineral formation as recorded by stable isotopes." *Minerals*, *12*(12), 1627. https://doi.org/10.3390/min12121627

minerals

MDPI

Article

Calcium Carbonate Hexahydrate (Ikaite): History of Mineral Formation as Recorded by Stable Isotopes

Michael J. Whiticar [1,*], Erwin Suess [2,3], Gerold Wefer [4] and Peter J. Müller [4,†]

[1] School of Earth and Ocean Sciences, University of Victoria, Victoria, BC V8W 2Y2, Canada
[2] GEOMAR Helmholtz Centre for Ocean Research Kiel, Wischhofstraße 1-3, 24148 Kiel, Germany
[3] College of Earth, Ocean, and Atmospheric Sciences, Oregon State University, Corvallis, OR 97330, USA
[4] MARUM Center for Marine Environmental Sciences, Universität Bremen, Leobener Straße 8, 28359 Bremen, Germany
* Correspondence: whiticar@uvic.ca
† Deceased.

Abstract: Calcium carbonate hexahydrate (ikaite) is a rare mineral that forms as metastable species in the organic-carbon-rich sediments of the King George Basin, Bransfield Strait, Antarctica, as a consequence of early diagenetic decomposition of organic matter under cold water (−1.4 °C) and high pressure (200 bar) conditions. Large crystals grow in the sediment immediately below the diagenetic transition between microbial sulfate reduction and methanogenesis at ~320 cm below sea floor (bsf). This process is reflected in the dissolved sulfate, total carbon dioxide, and methane concentrations, as well as in the carbon, hydrogen, and oxygen isotope chemistries of the interstitial fluids and dissolved gases of the host sediment. The ikaite crystal faithfully records in its zonal structure the changing carbon isotope ratio of the total dissolved carbon dioxide pool as it gradually diminishes during methanogenesis ($\delta^{13}C_{ikaite}$ = −17.5 to −21.4‰). These changes in the crystal's host environment follow general Rayleigh carbon isotope fractionation. The oxygen isotopes of the ikaite carbonate ($\delta^{18}O_{ikaite}$ = 1.46 to 4.45‰) also show a strong zonal distribution, unrelated to temperature of formation, but perhaps controlled by the degree of recrystallization of ikaite to calcite. The crystal water of the ikaite is depleted 11‰ in $^{2}H/^{1}H$ (VSMOW) relative to the coexisting interstitial water, which is in excellent agreement with the isotope fractionation of other hydrated minerals. In addition to the in situ temperature and pressure, nucleation of the ikaite crystals in the Bransfield Basin sediments may be induced by the high alkalinity, high phosphate concentrations, and dissolved organic compounds. Intense microbial metabolism generates such compounds; of these, aspartic acid and glutamic acid may play an important role, as they do in biological and extracellular carbonate mineral precipitation. All indications are that low temperatures (such as of polar environments), high calcium carbonate supersaturation caused by interstitial methanogenesis, and a sufficiently large supply of dissolved phosphate and amino acids favor metastable ikaite formation. These conditions, modified by recrystallization, may be preserved in calcite glendonites, thinolites, and other calcitic pseudomorphs derived from ikaite and found throughout the ancient sedimentary record.

Keywords: ikaite; calcium carbonate hexahydrate; glendonite; Bransfield Strait; diagenesis; stable isotope; geochemistry; palaeoclimate

check for updates

Citation: Whiticar, M.J.; Suess, E.; Wefer, G.; Müller, P.J. Calcium Carbonate Hexahydrate (Ikaite): History of Mineral Formation as Recorded by Stable Isotopes. *Minerals* **2022**, *12*, 1627. https://doi.org/10.3390/min12121627

Academic Editors: Gabrielle J. Stockmann and Juan Diego Rodríguez-Blanco

Received: 27 September 2022
Accepted: 13 December 2022
Published: 17 December 2022

Publisher's Note: MDPI stays neutral with regard to jurisdictional claims in published maps and institutional affiliations.

Copyright: © 2022 by the authors. Licensee MDPI, Basel, Switzerland. This article is an open access article distributed under the terms and conditions of the Creative Commons Attribution (CC BY) license (https://creativecommons.org/licenses/by/4.0/).

1. Introduction

Calcium carbonate hexahydrate is a monoclinic, hydrated carbonate mineral ($CaCO_3 \cdot 6H_2O$; Dana Class: 15.01.04.01 Hydrated Carbonates; Nickel–Strunz classification: 05.CB.25) that is composed of Ca–CO_3 surrounded by six water molecules [1,2]. Calcium carbonate hexahydrate has been known from synthesis studies since the 1800s [3–5]. Naturally occurring calcium carbonate hexahydrate is less commonly reported and was originally discovered by Hans Pauly in Ikka Fjord, Ivigtut, Greenland [6], after which the

mineral name ikaite was applied (granted by International Mineralogical Association in 1963). Natural occurrences of ikaite are severely limited under Earth's surface conditions because its stability is favored by high pressures and low temperatures. Yet, in many environments, ranging from deep-sea trenches and fans [7,8], glacial fjords and shelves [6,9], to polar basins [10–14], ikaite forms as a metastable species, sometimes in preference over calcite and aragonite. The formation of ikaite may be favored over calcite and aragonite by a combination of calcium-rich, high-alkaline fluids with elevated calcite-inhibiting inorganic compounds, e.g., calcium, magnesium, phosphate, sulfate [15,16], and/or organic additives [2,17–24].

Ikaite also occurs in a wide range of other environments, including sea ice [25–29], speleothems [30], alkaline springs or lakes [21,31,32], in riverbeds (due to anthropogenic pollution [33]), and in foods (e.g., frozen shrimp [34,35] and cheese [36]).

The ancient sedimentary record contains ample evidence, such as in glendonites, that ikaite was present in low-latitude marine sediments from the Neoproterozoic Era [37,38] Ediacaran Period (635–538.8 Mya) through to the present. It is now established that calcite hexahydrate is the precursor of thinolites, glendonites, gennoishi, jarrowites, and other calcitic pseudomorphs, nodules, and concretions seen worldwide. Some Ediacaran glendonites are silicified, replacing calcitic pseudomorphs that had resulted from earlier replacement of ikaites; new data suggest that they formed during an early Ediacaran cold period [39–46].

We examine here the detailed conditions of ikaite formation and its use as a paleoenvironmental indicator based on interstitial fluid chemistry, isotopic signatures, and diagnostic amino acid compositions retained in the crystal structure. Earlier, we reported calcite hexahydrate forming in recent organic-carbon-rich sediments of the King George Basin, Bransfield Strait, Antarctica [10], (Figure 1). In this back-arc basin, large, euhedral, monoclinic crystals of ikaite were repeatedly found in sediments from water depths of >1900 m. The crystals were chemically similar, as well as optically and structurally identical to the mineral ikaite from the Ikka Fjord, Greenland [6,9,47], hence our usage of this mineral name.

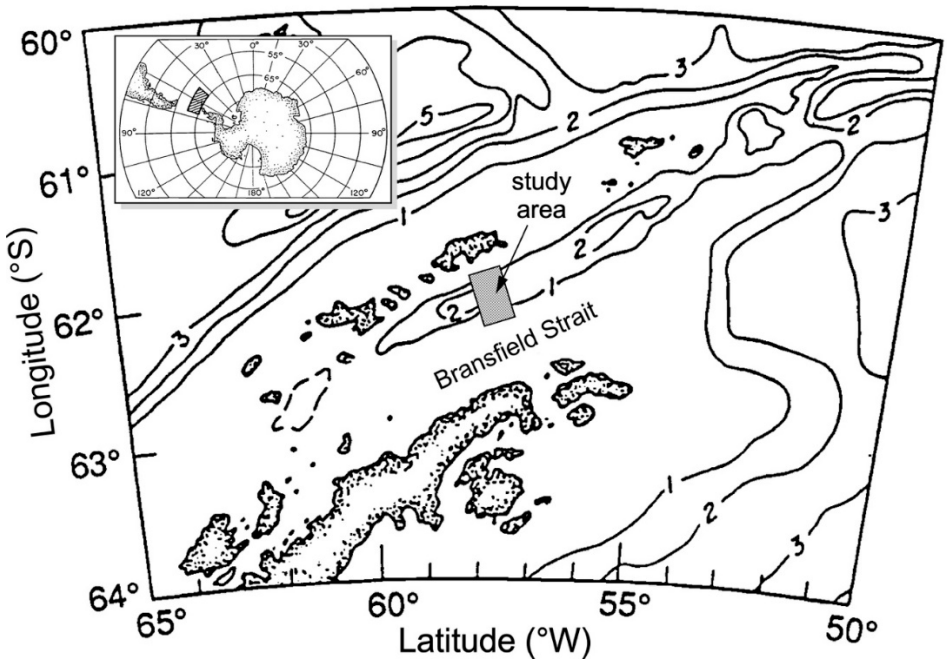

Figure 1. Location map of Bransfield Strait study area. Numbers 1, 2, 3, etc., on the map are 1000 m isobaths.

In the King George Basin, we postulate that ikaite forms as a consequence of diagenetic decomposition of sedimentary organic matter. These conditions are reflected in the

interstitial fluid chemistry, including the carbon, oxygen, and hydrogen isotope ratios and the dissolved methane in the host sediment. As we discuss, the ikaite crystals grow in the sediment just beneath the diagenetic transition zone between microbial sulfate reduction and hydrogenotrophic methanogenesis at ~320 cm below seafloor (bsf). We also postulate that the ikaite growth is limited within the methanogenic zone to a ~65 cm depth interval from ~320 to 385 cm bsf. With our limited radiometric dating, this 65 cm interval corresponds to an ikaite growth period of <1000 years. The preferential formation of ikaite over other carbonate polymorphs, e.g., calcite, aragonite, and vaterite, is predicated on the in situ pressure and temperature (>200 bar and −1.4 °C, respectively). Nucleation may be induced by organic compounds, rich in acidic amino acids, which result from intense methanogenic bacterial metabolism, but also from a range of other potential inhibitors presented in the paper.

This study was undertaken with the RV Polarstern in the area of the initial discovery in the King George Basin, Bransfield Strait, Antarctic [10,48]. Interstitial fluids and gases were obtained and analyzed from (1) a giant box core, ANT 1138-4 [49,50], that penetrated to a sediment depth of 1225 cm bsf; (2) a 760 cm gravity core, ANT 1327-1; (3) a 50 cm short box core, ANT 1324-2; and (4) a single sample from a 2050 cm giant piston core, ANT 1344-1. The water depth at ANT 1138-4 was 1985 m, and ikaite crystals were encountered repeatedly between 714 and 727 cm bsf, suggesting that ikaites may occur as an extensive subsurface pavement of crystals. The Bransfield Strait is an active back-arc basin; its morphotectonic setting is described by [51–53]. For comparison, two samples of glendonite samples from Spitzbergen and the Canadian Arctic were also collected and analyzed as a C–O isotope profile. Furthermore, we report on additional ikaite, glendonite, thinolites, and other pseudomorph samples from the U.S. (Hoh Fm, Astoria Fm, Arctic, DSDP 583 and 584) and compare their C–O isotope compositions with the existing worldwide data on glendonites.

2. Methods

2.1. Shipboard Analyses

Interstitial waters from the mineral's host sediment of the three stations were collected by pressure filtration at the temperature of the bottom water close to 0 °C with a technique similar to that described by [54]. The total dissolved carbon dioxide (DIC) was determined by acidification, He-stripping of the interstitial waters, and online CO_2 gas chromatography, while dissolved sulfate was determined gravimetrically as $BaSO_4$, and dissolved ammonium was measured photometrically. The results are reported in units of millimoles (mM) of interstitial water (Table 1). They represent a composite downcore dataset with increased frequency of samples near the sediment–water interface, the sulfate reduction zone (SRZ)–methanogenic zone (MZ) transition, and the ikaite crystal horizon. Note, for simplicity, the species charges are understood and not added, e.g., NH_4^+ is reported as NH_4.

Hydrocarbon gases were extracted from fresh sediment core sections using a vacuum/acid degassing procedure [55]. Gas concentrations were quantified by FID gas chromatography and are reported in parts per billion (ppb wt.), i.e., as weight of the hydrocarbon gas per weight of wet sediment (Table 1). Interstitial water samples for stable isotope measurements were drawn into vacutainers and treated with mercuric chloride. Mineral fragments of ikaite, generally from the crystal surface, were placed in glass ampoules, flushed with nitrogen, and sealed rapidly.

Table 1. Chemical composition of interstitial fluids and gases in Bransfield Strait cores ANT 1138-4 (1), 1324-2 (2), and 1327-1 (3).

Depth	Core	DIC	SO_4	NH_4	PO_4	Ca	Mg	Mg:Ca	CH_4	$\delta^{13}CH_4$	$\delta^{13}CO_2$	$\delta^{2}H$-CH_4	$\delta^{2}H$-H_2O	$\delta^{18}O$-H_2O
cm	no.	mM	mM	mM	mM	mM	mM	(mol)	ppb wt.	‰, VPDB	‰, VPDB	‰, VSMOW	‰, VSMOW	‰, VSMOW
seawater		2.2	28.00	0.00	0.003				1		−0.1		0.0	0.0
0.5	2	4.2	27.33	0.14										
3.5	2	5.4	26.61	0.18										
6.5	2	6.6	26.11	0.20										
10.0	3	6.8	25.66	0.34	0.075	10.40	52.62	5.1	39	−69.5				
12.0	2	7.6	25.58	0.23										
15.5	2	9.5	24.82	0.23										
20.5	2	10.6	24.36	0.27										
25.5	2	11.8	22.67	0.61	0.082				32	−51.4	−18.2			
26.0	3	12.4	23.95	0.30		10.40	52.83	5.1						
37.5	2	14.5	22.51	0.34										
51.0	3	18.0	20.46	0.85	0.207	10.53	52.13	5.0	39	−58.9	−19.8			
78.0	1	17.8	19.94	0.61	0.131						−18.4		−4.9	0.0
112.0	3	29.1	14.45	1.02	0.360	10.70	51.39	4.8	50	−60.3	−22.8			
133.0	1	26.4	15.12	1.02	0.191	9.64								
203.0	3	39.5	5.92	1.76	0.262	8.83	50.20	5.7			−20.6			0.0
235.0	1	42.9	5.54	1.82	0.542	10.35			82	−59.3				
322.0	3	53.3	0.20	2.23	0.509	9.60	49.62	5.2	7340	−99.7	−23.7			
366.0	1	55.1	0.10	2.32	0.387	9.21								
370.0	3	54.6	0.05	2.38	0.522	9.98	50.36	5.0	14890	−100.7				
412.0	3	56.6	0.05	2.57	0.426	9.78	50.73	5.2	17465	−101.9				
431.0	1	57.9	0.05	2.70	0.275	8.38					−17.5		−7.0	−0.4
468.0	3	55.8	0.05	2.74	0.364	9.38	50.61	5.4	22540	−100.7				
512.0	3	55.7	0.05	2.74	0.253	8.53	50.57	5.9	46380	−100.2				
520.0	1	59.2	0.05	2.96	0.284	8.33								
552.0	3	56.6	0.05	2.92	0.331	8.50	51.96	6.1	28740	−98.4				
633.0	3	55.7	0.05	3.07	0.224	7.30	52.17	7.1	16950	−94.9				
658.0	1	59.7	0.05	3.09	0.235				10720	−95.8		−200.0		−0.1
692.0	1	59.7	0.05	3.20	0.215	6.82					−13.7			
728.0	3	58.7	0.05	3.12					8564	−90.3				
752.0	1	59.1	0.05	3.20	0.185						−11.9		−5.2	−0.1
753.0	3	57.9	0.05	3.22	0.157	7.50	53.82	7.2	15480	−88.5				
790.0	1	60.7	0.05	3.20	0.158	5.93								
812.0	1	60.0	0.05	3.20	0.158	5.71			7395	−93.2	−11.7	−205.0		−0.1
908.0	1	59.8	0.05	3.20	0.134	5.83								
1033.0	1	59.8	0.05	3.48	0.101	6.48					−7.9		−5.6	−0.1
1111.0	1	62.5	0.05	3.67	0.106	7.08			4338	−89.2		−198.0		
1162.0	1	64.2	0.05	3.87	0.101				5247	−86.5	−5.7	−194.0		−0.1

2.2. Shore-Based Analyses

Isotope measurements were made of dissolved inorganic carbon, DIC ($^{13}C/^{12}C$), interstitial water ($^{18}O/^{16}O$ and $^{2}H/^{1}H$), and methane ($^{13}C/^{12}C$ and $^{2}H/^{1}H$) on variably spaced samples throughout the composite depth of coring. The crystal-hydration water of "in vitro" decomposed ikaite mineral fragments, collected and kept in glass ampoules, were analyzed for $^{2}H/^{1}H$ ($^{18}O/^{16}O$ of the hydration water was not measured). The calcium carbonate residue of bulk ikaite after decomposition was analyzed for $^{13}C/^{12}C$ and $^{18}O/^{16}O$ ratios. In addition, a microsampling traverse of 7 points was made with a fine drill across the lateral growth axis of a 43 mm long × 17 mm wide ikaite single crystal (sample ID K735) and, similarly, at 3 points along the surface of the crystal in the direction of longitudinal growth (c*-axis) [47,56]. For comparison, similar microsampling traverses were made on two glendonite samples (calcite pseudomorphs) from Spitzbergen and Canada. These microsamples were analyzed for $^{13}C/^{12}C$ and $^{18}O/^{16}O$ of the calcium carbonate.

2.3. Isotope Methods

The interstitial H_2O was reduced to hydrogen for $^{2}H/^{1}H$ measurement by freezing the H_2O over onto zinc-filled 6 mm glass tubes, which were evacuated, sealed, and heated to 460 °C [57]. In a similar manner, for the H_2O released from the ikaite fragments, decomposition was accelerated by slight heating (<40 °C), was frozen over (under vacuum) onto the zinc tubes, and then reduced to hydrogen gas for $^{2}H/^{1}H$ measurement. The DIC in the interstitial waters was released by acidification and collected at 25 °C for C- and O-isotope determinations. The bulk and traverse-sampled calcium carbonates of the ikaite were prepared for C- and O-isotope ratios by the conventional H_3PO_4 acidification method of [58].

Methane was partitioned by gas chromatography (GC) and then combusted with CuO at 880 °C [59]. The $^{13}C/^{12}C$ of the resultant CO_2 was measured directly by isotope ratio mass spectrometry (IRMS). The H_2O from the methane combustion was subsequently reduced on zinc, and the $^{2}H/^{1}H$ was measured on the evolved hydrogen gas by GC-IRMS. The stable carbon and hydrogen isotope results (Table 1) are reported in the usual δ-notation of $\delta^{2}H$, $\delta^{13}C$, and $\delta^{18}O$, whereby

$$\delta^{n}X = \left(\frac{{}^{n}R_{sa} - {}^{n}R_{st}}{{}^{n}R_{st}} \right) \times 10^{3} \quad (1)$$

and R_{sa} are the $^{2}H/^{1}H$, and $^{2}H/^{1}H$ and $^{18}O/^{16}O$ ratios in the sample relative to R_{st}, the corresponding ratios in the standards Vienna Peedee belemnite (VPDB) and Vienna standard mean ocean water (VSMOW). The isotope fractionation factors (α_{A-B}) are defined as

$$\alpha X_{A-B} = (R_A/R_B) = \frac{(\delta_A + 10^3)}{(\delta_B + 10^3)}, \quad (2)$$

whereby the isotope having the larger mass is more concentrated in chemical species A than in B. This relationship generally implies isotopic equilibrium, which may not necessarily be the case in all the reactions discussed here.

2.4. Amino Acids

For the analysis of amino acids, 135 mg of the homogenized, dry, ikaite material was weighed into heavy-walled glass ampoules, flushed with purified nitrogen for 3 min after adding 2 mL of 6N HCI, sealed, and then hydrolyzed at 110 °C for 22 h. Appropriate amounts of norleucine (1.25 mmole) were added as internal standard prior to hydrolysis [60]. The hydrolysate was evaporated to dryness at reduced pressure and the residue taken up in 2 mL of sodium citrate buffer (pH 2.0, 0.18 N Na^{+}). Aliquots of 250 µL were injected into an automatic amino acid analyzer (Biotronik) for separation and detection.

Amino acids were separated by ion exchange chromatography using a sodium citrate 4-buffer system for elution, the q-phthalaldehyde method for detection [61,62], and a computing integrator (Spectra Physics 4100) for peak integration and quantification [63]. The concentrations of amino acids were calculated from norleucine recovery, which ranged from 78 to 90 % in similar analytical runs. Amino sugars were not quantified here.

3. Diagenetic Environment

3.1. Nutrient Stoichiometries

The unconsolidated sediments from the King George Basin, in which the ikaites are found, are organic-rich, rapidly deposited, and undergo diagenesis in strongly anoxic conditions. Dissolved sulfate decreases rapidly below the water–sediment interface downcore, from a normal seawater concentration of 28 mM to exhaustion at ~320 cm bsf (Figure 2, Table 1) as it is utilized by sulfate-reducing bacteria (SRB) in the oxidation of organic matter. In this initial depth interval of sulfate consumption, methane concentrations are low, at low background levels of <100 ppb wt. (Figure 2, Table 1). Following the depletion of dissolved sulfate at ca. 320 cm bsf, methane concentrations quickly increase up to >46 ppm wt. The depth separation of the sulfate reduction and methane formation zones (SRZ and MFZ) is typical for anaerobic marine sediments that are rich in organic carbon [64], $\delta^{13}C_{CH4}$, and $\delta^{2}H_{CH4}$ measurements, i.e., from −95.8 to −83.8‰ and from −200 to −194‰, respectively (Figure 2, Table 1). This indicates that the methane is of archaebacterial origin and a product of the hydrogenotrophic methanogenic pathway [64]. A further consequence of organic matter decomposition is the steady regeneration of dissolved DIC and ammonium (Figure 2, Table 1). Ammonium rapidly accumulates up to 2 mM in the sulfate-reducing zone and continues to rise, albeit more slowly, in the methanogenic zone to over 3.88 mM at the greatest depth cored (2055 cm bsf). DIC also increases rapidly in the SRZ from 2.2 mM to 53 mM at 320 cm bsf. However, in contrast to the ammonium, its concentration below the SRZ increases only slightly to a maximum of 64 mM at 1162 cm bsf. In the sulfate-reduction zone, dissolved phosphate increases from seawater values (~2 µM) to over 0.5 mM (Figure 2) but then drops steadily below the SRZ to 0.1 mM at 1162 cm bsf.

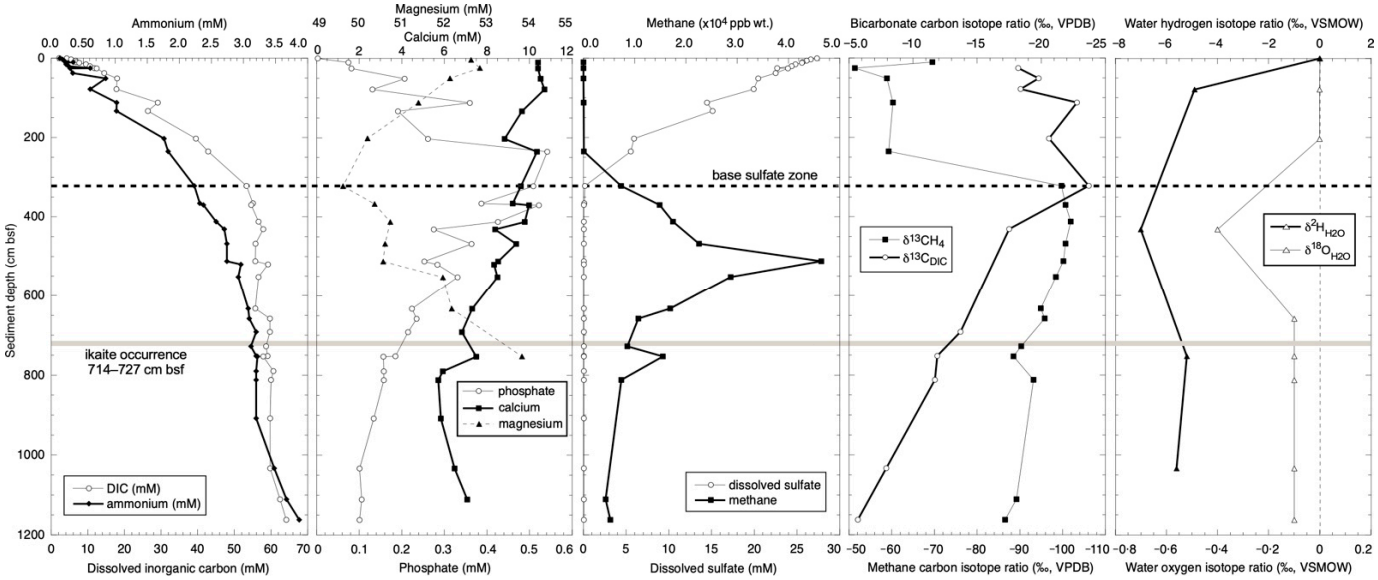

Figure 2. Depth distributions of dissolved nutrients, sulfate, calcium, magnesium, methane, stable carbon, oxygen, and hydrogen isotopes of dissolved inorganic carbon, methane, and interstitial water, as composite from three Bransfield Strait cores ANT 1138-4, 1324-7, and 1327-1.

The depth distribution of dissolved DIC is controlled by various and sometimes competing diagenetic processes that can be followed using stable isotope signatures of the gas and fluid reservoirs. To understand ikaite formation in the King George Basin, it is

essential to first discuss the dissolved DIC habitat from which the mineral is derived. The initial rise in DIC to 53 mM (Figure 2) is largely due to organic matter remineralization related to bacterial sulfate reduction in the SRZ. This is evident in the highly significant negative stoichiometric correlation between DIC and SO_4, and between NH_4 and SO_4 (core ANT 1138-2, Equations (3) and (4), Figure 3):

$$\text{DIC (mM)} = -1.79\ SO_4\ \text{(mM)} + 53.5;\ r = 0.997 \quad (3)$$

and between ΔNH_4 and $-\Delta SO_4$ (Figure 3):

$$NH_4\ \text{(mM)} = -0.079\ SO_4\ \text{(mM)} + 2.26;\ r = 0.993 \quad (4)$$

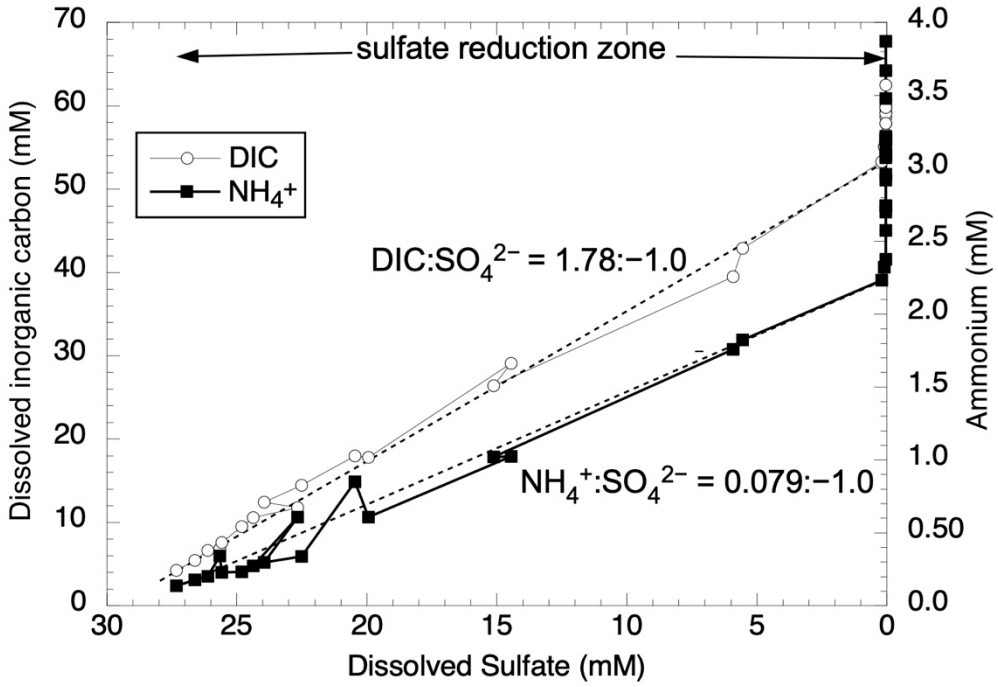

Figure 3. Linear stoichiometric relationship between dissolved inorganic carbon (DIC) and ammonium with dissolved sulfate in core ANT 1138-2. The DIC and ammonium continue to increase below the SRZ, as shown.

The slight deviation from the ideal regeneration ratio of $\Delta DIC:-\Delta SO_4 = 2:1$ suggests that the anaerobic oxidation of methane by sulfate-reducing bacteria consumes sulfate at the base of this zone [64,65]. Below 320 cm bsf and within the zone of methanogenesis, the input to the DIC reservoir by remineralization of the organic matter slightly exceeds the depletion of the DIC pool by methanogenesis. This is reflected by the continued slight increase in DIC observed at depth, whereas ammonium continues to increase with depth (Figure 2).

The depth distribution of phosphate in core ANT 1138-2 is very different from both DIC and NH_4. In the SRZ, phosphate linearly tracks the increased ammonium due to organic matter remineralization, up to a maximum of 0.39 mM (Figure 4), with the stoichiometry of

$$NH_4\ \text{(mM)} = 0.155\ PO_4\ \text{(mM)} + 0.018;\ r = 0.989. \quad (5)$$

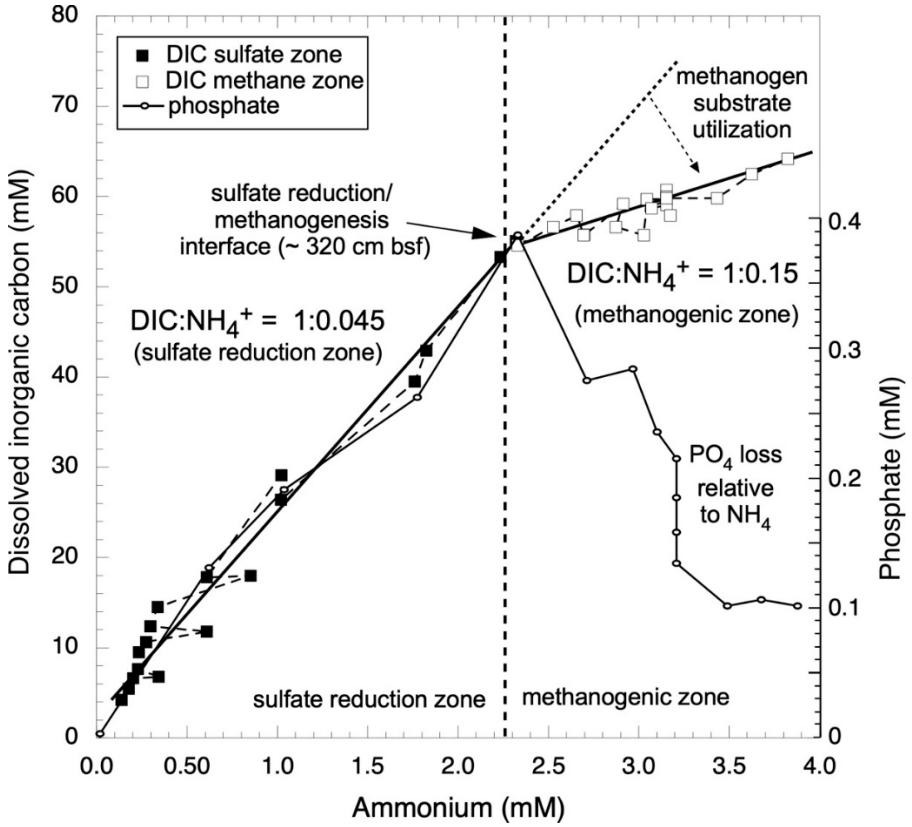

Figure 4. Stoichiometry between dissolved inorganic carbon (DIC) and phosphate with ammonium in core ANT 1138-2, illustrating the linear C:N and N:P relationships within the diagenetic sulfate-reduction zone (SRZ). The change in C:N beneath the SRZ is due to methanogenic uptake of DIC. The dramatic loss in phosphate relative to ammonium beneath the SRZ is clearly evident.

However, beneath the SRZ, phosphate decreases continually in concentration down to 0.1 mM. This bifurcated relationship is illustrated in Figure 4, with the clear departure of phosphate from both NH_4 and DIC beneath the SRZ. On the other hand, phosphate tends to track the loss of calcium below the SRZ (Figure 5), which may be due to the uptake by calcium orthophosphates. The molar ratio of phosphate tracking Ca loss below the SRZ is almost 1:1, suggesting such a process.

Some Neoproterozoic strata, potentially associated with the "Snowball Earth" [66], also contain glendonites, e.g., Dalradian slates and metalimestones, Scotland [37,38], and some lithologic units in the early Doushantuo, China, which are dominated by phosphorites [45,46].

3.2. Carbon Isotope Variation in DIC

The carbon isotope ratio of DIC ($\delta^{13}C_{DIC}$) measured downcore shows an interesting isotopic reversal (Figure 2). Firstly, there is an excursion in $\delta^{13}C_{DIC}$ from 0‰ to −23.7‰ between the sediment–water interface and the base of the SRZ (Table 1). Beneath the SRZ, $\delta^{13}C_{DIC}$ is continually enriched in ^{13}C, from −23.7‰ to −5.7‰, with increasing sediment depth. This characteristic isotope depth distribution can be related primarily to two separate diagenetic processes: (1) isotopic mixing of different bicarbonate sources during remineralization, and (2) isotopically fractionated removal during methanogenesis. These are described below.

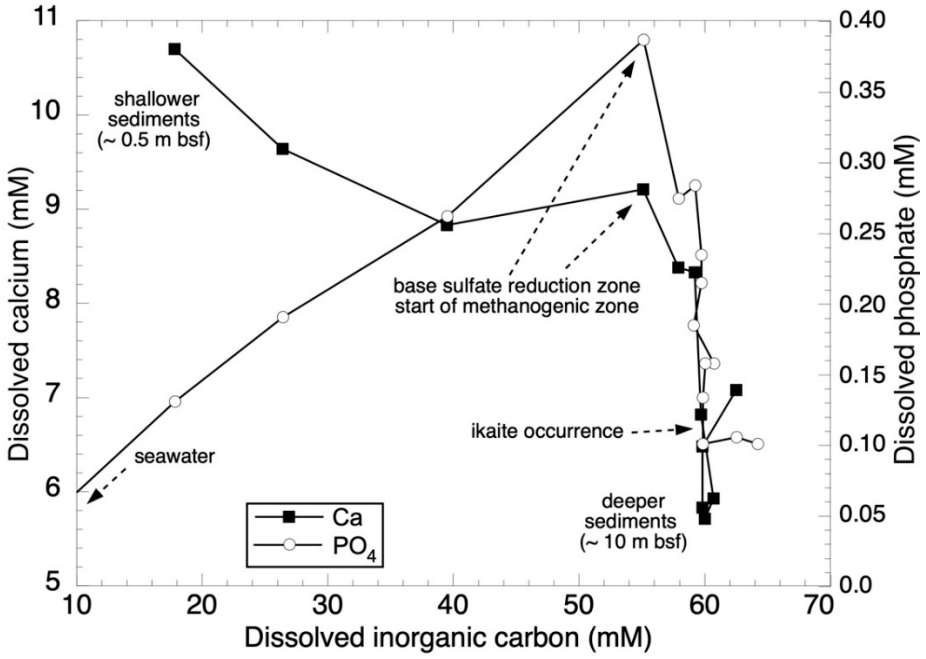

Figure 5. Stoichiometry between dissolved calcium and phosphate with dissolved inorganic carbon (DIC) in core ANT 1138-2. DIC:P has a linear relationship within the diagenetic sulfate-reduction zone (SRZ), but dramatically departs, as indicated at depths beneath the base of the SRZ. Calcium shows little change in the SRZ, then also decreases and tracks phosphate at depths below the SRZ. The sediment depth of ikaite occurrence is shown.

3.2.1. Linear Isotope Mixing

Between the sediment surface and the base of the SRZ at 320 cm bsf, the $\delta^{13}C_{DICtotal}$ represents a mixture of dissolved inorganic carbon from incorporated bottom seawater (DIC_{sw}, 2.2 mM, $\delta^{13}C_{DICsw} \sim 0‰$) and DIC_{org} ($\delta^{13}C_{DICorg} \sim -24‰$) that has been derived from the decomposition of organic matter ($\delta^{13}C_{org} \sim -25‰$) in the sediments through diagenesis. The resultant carbon isotope composition of this mixture is approximated by the linear mixing in Equation (6):

$$f_{total} \cdot \delta^{13}C_{DICtotal} = f_{sw} \cdot \delta^{13}C_{DICsw} + f_{org} \cdot \delta^{13}C_{DICorg}, \quad (6)$$

where f_a is the fraction of the concentration (mM) and f_{total} is $f_{sw} + f_{org}$.

The isotope mixing line, drawn in the SRZ (Figure 6, right panel), is generated using the actual measured DIC concentration (f_{total}) increasing with depth. Although there is more variability in the actual measured values, these mixing-model values adequately describe the $\delta^{13}C_{DICtotal}$ distribution down to near the base of the SRZ.

3.2.2. Kinetic Isotope Effects Associated with Methanogenesis

Beneath the SRZ, deeper than 360 cm bsf, the observed $\delta^{13}C_{DIC}$ profile is modulated by carbon isotopic fractionation due to methanogenesis. The higher conversion rate by methanogens of $^{12}C_{DIC}$ over $^{13}C_{DIC}$ into methane leads to a substantial shift to ^{13}C-enriched values in the carbon isotope ratio of residual DIC in the MFZ (Figure 6) [67,68]. This intense, archaebacterial-mediated kinetic isotope effect is easily observed in the accumulation of methane in the sediments that is depleted in ^{13}C, i.e., $\delta^{13}C_{CH4} \sim -100‰$ (Figures 2 and 6, Table 1).

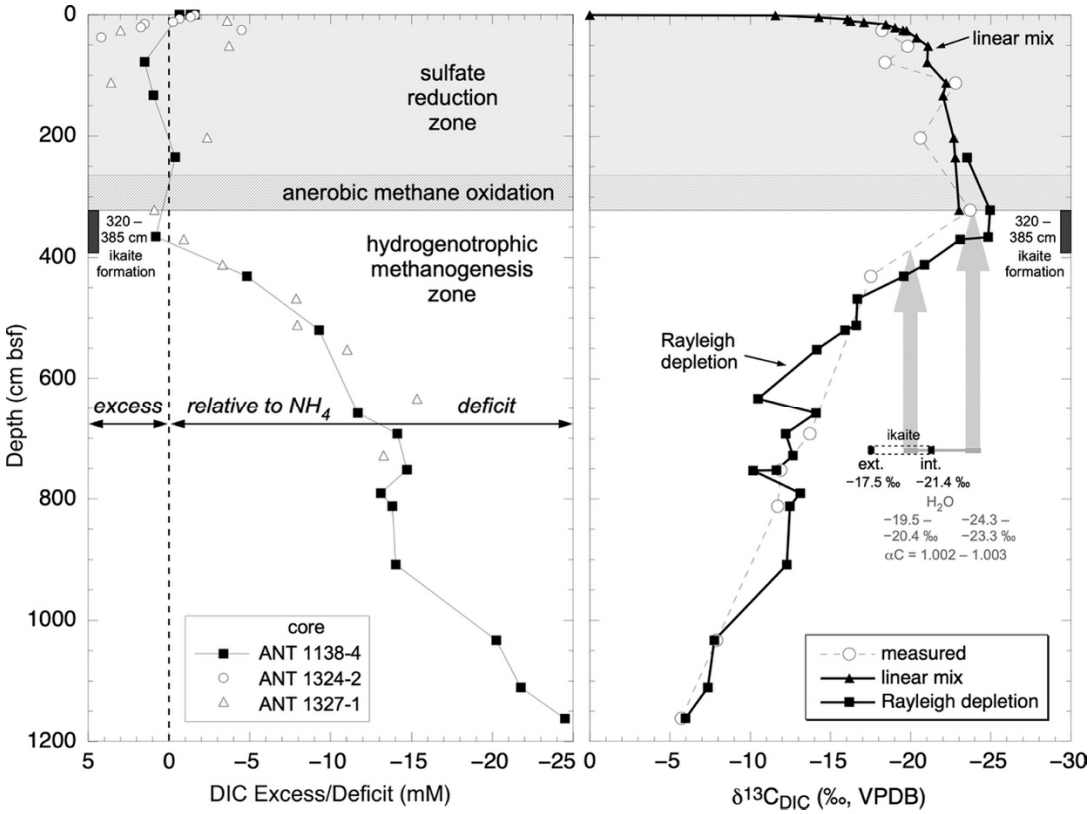

Figure 6. (Left panel) Calculated DIC excess and deficit (beneath SRZ) based on a conservative DIC:NH_4 stoichiometry model, assuming that the NH_4 concentration is only affected by addition through remineralization and the reference C:N is 1:0.045 (Equation (8)) in the SRZ. The loss in DIC is due to uptake by methanogens. (Right panel) Measured (open circles) and modeled $\delta^{13}C_{DIC}$ depth distributions using a combination of: (1) mixing line in the SRZ (closed triangles), which indicates DIC input from microbial sulfate reduction and buried oceanic DIC (Equation (5)), and (2) Rayleigh-based carbon isotope fractionation of DIC by methanogen utilization (Equations (7) and (9)) beneath the SRZ. The current depth of ikaite occurrence is shown along with the measured profile range in $\delta^{13}C_{ikaite}$ along with the range in $\delta^{13}C_{DIC}$ expected based on the $\alpha C_{ikaite\text{-}H2O}$ range of 1.002 to 1.003. The "ext." and "int." are the $\delta^{13}C_{ikaite}$ for the interior and exterior of the crystal (Section 4.3).

Carbon isotope fractionation during methanogenesis by carbonate reduction in a closed system leading to DIC enriched in ^{12}C can be described by the general Rayleigh-type equation [69]:

$$R_t = R_o \cdot f(\alpha_c - 1), \quad (7)$$

where R is the $^{13}C/^{12}C$ ratio of the initial DIC (R_o) and the residual DIC (R_t) of the fraction DIC remaining reservoir (f) as f goes from 1 to 0. The Rayleigh equation, approximated by [70], has been converted to δ-notation as

$$\delta^{13}C_{DIC_t} = \left(\delta^{13}C_{DIC_i} + 10^3\right) f^{(\alpha-1)} - 10^3, \quad (8)$$

where $\delta^{13}C_{DIC(i)}$ is the initial DIC carbon isotope value (−24‰), $\delta^{13}C_{DIC(t)}$ is the carbon isotope value of the DIC reservoir at time t, and f is the fraction of the DIC precursor pool remaining after uptake by hydrogenotrophic methanogenesis and $\alpha C_{methane\text{-}DIC}$. The difficulty in solving Equation (8) lies in the proper estimation of the DIC fraction that has been removed from the precursor pool during bacterial carbonate reduction, i.e., $1 - f$. As a first approximation, this DIC fraction can be estimated by comparing the DIC with the corresponding ammonium concentration that accumulates in the interstitial water, as described below.

The accumulation of ammonium may be assumed to represent the degree of organic matter remineralization at each depth interval. This is generally true because ammonium remains largely unaffected in these sediments by secondary reactions, such as precipitation or further metabolism. Admittedly, absorption of minor amounts ammonium will introduce some error into this estimation. However, comparison with the phosphate concentrations reveals that this error is, in fact, small. In the SRZ, where the DIC is unaffected by methanogenesis, the DIC is stoichiometrically related to NH_4 as follows:

$$\text{DIC (mM)} = 22.2\ \text{NH4 (mM)} + 2.81;\ r = 0.989, \quad (9)$$

which corresponds to a molar DIC:NH4 ratio of 1:0.045 (closed symbols in Figure 4), and a Redfield-based C:N of 105:4.7. Clearly, the amount of ammonium regenerated compared to DIC is less than that predicted by the normal diagenetic model. In the zone of methanogenesis (open symbols in Figure 4), the molar DIC:NH_4 ratio shifts markedly to a value of 1:0.21, which corresponds to a C:N of 22.1:4.7. This decrease in C:N is a direct consequence of the combined effects of: (1) the continued addition of ammonium and bicarbonate to the interstitial fluid by remineralization and (2) the preferential removal of DIC by methanogens during methanogenesis via the hydrogenotrophic pathway.

The predicted DIC concentration, i.e., that which would have been present in the deeper sediments (>320 cm bsf) without any removal by methanogenesis via carbonate reduction, can be calculated directly from the ammonium concentration using Equation (9). To do this, we assume that the release of DIC from the metabolizable organic matter in the methanogenic zone (prior to methanogenesis) follows the same C:N regeneration ratio as that observed in the SRZ, i.e., DIC:NH_4 = 1:0.045 (Figures 4 and 6, left panel). We also assume that the ammonium concentration is only affected by addition through remineralization. The difference between the predicted and the measured DIC concentrations in the methanogenic zone is therefore the fraction of bicarbonate consumed as a result of methanogenesis or other DIC removal. If there is more DIC than predicted by the corresponding NH_4, then the DIC is in excess. The opposite situation is a DIC deficit. As shown in Figure 6 (left panel), there is a clear and strong DIC deficit within the zone of methanogenesis that increases from 0 at the upper boundary (~350 cm bsf) to 24.5 mM at the base of the core ANT 1138-4 (1162 cm bsf). This corresponds to a change in the DIC reservoir with depth from f = 1.0 to 0.72, wherein

$$f = \text{DIC}_{\text{measured}} / \text{DIC}_{\text{predicted}}. \quad (10)$$

Using Equation (8) and taking $\delta^{13}C_{DIC(i)} = -24‰$ and $\alpha C_{\text{methane-DIC}} = 1.06$ for hydrogenotrophic methanogenesis [64], the change with depth for the predicted $\delta^{13}C_{DICt}$ can be calculated. Figure 6 (right panel) shows that this predicted change in $\delta^{13}C_{DIC}$ of the residual DIC reservoir due to methanogenesis adequately models the actual measured $\delta^{13}C_{DIC}$ profile in the methanogenic zone. Calcium carbonate hexahydrate precipitation is apparently not a major influence on the $\delta^{13}C_{DIC}$, nor on the magnitude of the DIC reservoir.

An independent confirmation for this DIC:NH_4 stoichiometric model is provided by the corresponding carbon isotopic shift in the accumulating methane ($\delta^{13}C_{CH4}$). The preferential ^{12}C depletion of the DIC substrate by methanogens enriches the remaining DIC in ^{13}C. As a consequence, the methane formed subsequently (deeper) becomes isotopically enriched in ^{13}C ($\delta^{13}C_{CH4}$ shifts from −101.9‰ to −86.5‰, Table 1). Figure 2 clearly demonstrates this parallel isotope tracking of $\delta^{13}C_{CH4}$ to $\delta^{13}C_{DIC}$ with increasing depth.

4. Calcium Carbonate Hexahydrate Precipitation

4.1. Ikaite Formation

It is our contention that the precipitation of the calcium carbonate hexahydrate was initiated at the base of the SRZ in response to increased carbonate supersaturation and inhibition of calcite and/or aragonite formation. Ikaite crystals formed in this zone were subsequently buried to greater depth, with some shorter-term additional growth. At the

prevailing conditions of the Bransfield Strait surface sediments, −1.4 °C and ca. 0.2 kbar, the metastable $CaCO_3 \cdot 6H_2O$ forms rather than calcite or aragonite. Based on the works of [20,21], ikaite at −1.4 °C would be the stable carbonate mineral only at pressures above 3.1 kbar. This metastable state accounts for the observed rapid decomposition at shipboard conditions of ikaite to vaterite, calcite or amorphous calcium carbonate, and H_2O [71,72]. It may also be responsible for the possible in situ recrystallization of the center portions of ikaites to sparry calcite and thus incipient pseudomorphism. Methanogenesis possibly initiates ikaite crystallization, analogous to that reported for calcite precipitation by other investigators [67,73–75]. The removal of bicarbonate by hydrogenotrophic methanogens, starting around 320 cm bsf, tends to raise the pH and thereby vastly increase the degree of supersaturation ($ICP/K_{sp} >> 1$). The resulting carbonate precipitation proceeds according to the following reaction:

$$Ca^{2+} + 2HCO_3^- + 3H_2O + 8H^+ \leftarrow CH_4 + CaCO_3 \cdot 6H_2O_{(s)}. \quad (11)$$

This possible association of ikaite and methane formation is supported indirectly by the close spatial relationship between the onset of methanogenesis and the suspected initial point of formation for the ikaite crystals.

An alternative explanation for the initiation of ikaite precipitation at the base of the sulfate zone is the accumulation of excess DIC, resulting from the anaerobic oxidation of methane. Methane, diffusing upward to the base of the sulfate zone, is consumed by methanotrophs, and returned in part to the interstitial water as DIC [64,65,76]. This anaerobic methane oxidation maintains the methane concentration at trace levels (<0.04 ppm) in the uppermost 300 cm bsf. The excess DIC in the methane oxidation zone is only weakly evident from the C:N stoichiometric model (Figure 4). The DIC concentration measured around 350 cm bsf, i.e., at the depth where significant methane consumption is occurring, is higher by only about 1 mM relative to that predicted from the ammonium concentration by Equation (9). This metabolic DIC derived from ^{12}C-enriched methane ($\delta^{13}C_{CH4} \sim -100‰$) should also be relatively enriched in ^{12}C. To some extent, such a ^{12}C-DIC isotope shift is observed around 300 cm bsf and fits the $\delta^{13}C_{DIC}$ model (Figure 6, right panel).

4.2. Radiocarbon Dating

Radiocarbon dates were obtained from two organic matter samples on an adjacent sediment core (Station 14882-278). Samples at 610 and 810 cm bsf yielded ages of 3560 yBP and 6530 yBP, respectively, giving an average sedimentation rate over this interval of ~0.67 mm y^{-1} (Erlenkeuser, 1984, unpublished data). Assuming that the ikaite crystal grew in the sediment depth interval of 320 to 385 cm bsf (65 cm), this average sedimentation rate corresponds to a crystal growth period of ~965 years. If the crystal growth was constant over this period, which certainly may not be true, then the estimated average growth rate for the ikaite crystal c*-axis (43 mm long) is ~0.045 mm/year. A single radiocarbon date on a carbonate sample of the ikaite outer rim ($\delta^{13}C_{ikaite} = -18.6‰$), collected at 720 cm bsf, gave a conventional, uncorrected age of 4600 yBP (Geyh, 1984, unpublished data). This, indirectly, provides the most recent age of the dissolved bicarbonate pool carbon incorporated into the ikaite. The corresponding age of the sediment at 720 cm bsf interpolated from the 610 and 810 cm bsf samples (3560 and 6530 yBP) was 5193 yBP. This rough agreement between the age dates of the sedimentary organic matter and interstitial fluid DIC precludes the possibility that substantial vertical transport and/or exchange in the interstitial water had occurred.

4.3. Carbon Isotope Zonation of Ikaite

An exceptionally large, 43 × 15 mm calcium carbonate hexahydrate crystal, collected from Antarctic sediment core ANT 1138-4, allowed us to verify the history of the ikaite mineral formation envisioned above. Carbon isotope profiles of subsamples, taken along a traverse of lateral crystal growth (Figure 7, Table 2), demonstrate the response of the calcium carbonate hexahydrate to the changing carbon isotope composition in the interstitial waters

from which it was derived. The carbon isotope ratio of the innermost (oldest) section of the crystal is that which is most depleted in ^{13}C ($\delta^{13}C_{ikaite}$ = −21.4‰, sample 7, Figure 7). Proceeding outwards to the younger growth, the carbon isotope ratio shifts progressively by +3.3‰ to ^{13}C-enriched $\delta^{13}C_{ikaite}$ values of ~−18.1‰ (samples 4 and 10, Figure 7). Analyses of three samples, drilled from the current outside crystal surface along the longitudinal growth axis, yielded $\delta^{13}C_{ikaite}$ values from −17.5‰ to −18.1‰ (samples 1, 2, and 3). These values agree with the outermost (youngest) samples from the transect. Assuming that the ikaite formed with constant isotope effects and in equilibrium conditions during its growth, then the $\delta^{13}C_{ikaite}$ shift of +3.9‰ (i.e., sample 1 vs. 7), from the innermost ikaite to its surface, indicates that the $\delta^{13}C_{ikaite}$ mirrors changes in $\delta^{13}C_{DIC}$ as the crystal grew, as indicated in Figure 7.

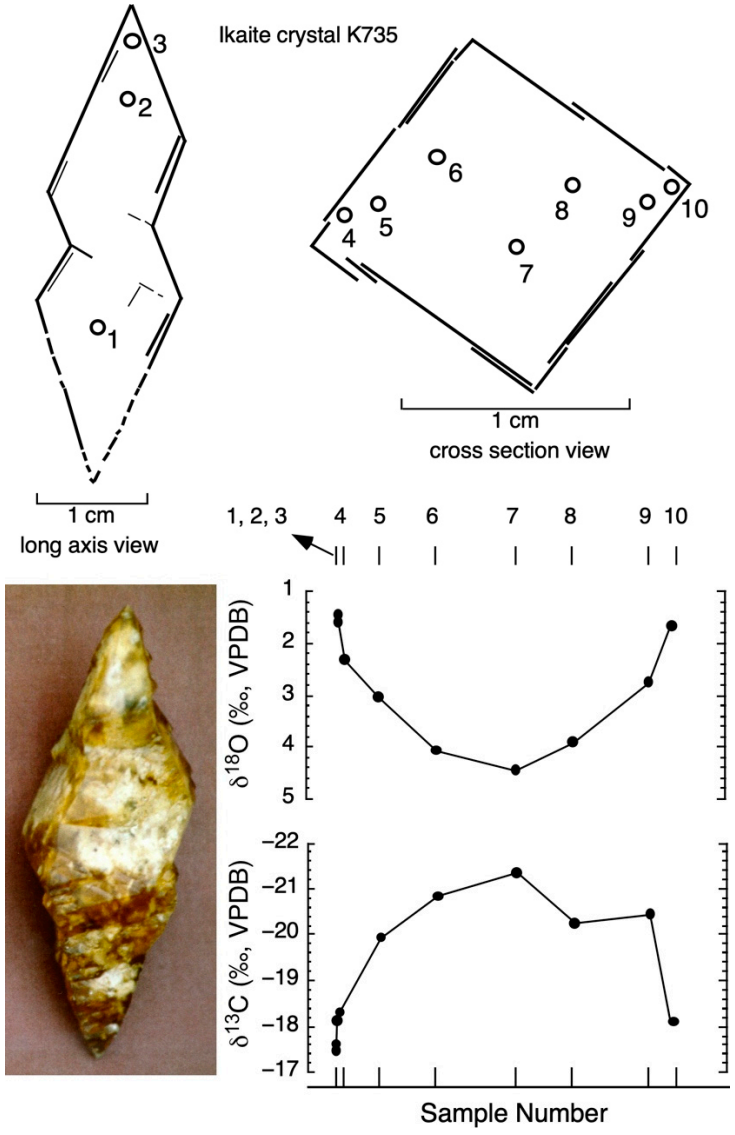

Figure 7. Carbon and oxygen isotope measurement traverse across ikaite crystal. Changes in $\delta^{13}C_{ikaite}$ reflect changes in $\delta^{13}C_{DIC}$ due to uptake of $^{12}C_{DIC}$ by methanogens during hydrogenotrophic methanogenesis. The changes in $\delta^{18}O_{ikaite}$ are possible due to kinetic isotope effects during the formation or the partial recrystallization of ikaite to calcite.

Table 2. Carbon and oxygen profiles across ikaite crystal (sample K735) and glendonites.

Sample No.	Distance across Crystal (mm)	$\delta^{13}C_{ikaite}$ Carbonate (VPDB)	$\delta^{18}O_{ikaite}$ Carbonate (VPDB)	Temperature (°C) (Grossman 2012)
		Bransfield Strait ikaite (sample K735)		
1	0.0	−17.49	1.58	8.71
2	0.0	−17.60	1.46	9.19
3	0.0	−18.10	1.60	8.63
4	1.6	−18.33	2.32	5.85
5	3.0	−19.95	3.04	3.19
6	5.6	−20.85	4.07	−0.39
7	9.1	−21.35	4.45	−1.65
8	11.6	−20.25	3.91	0.15
9	14.9	−20.46	2.75	4.25
10	15.9	−18.10	1.67	8.36
		Spitzbergen glendonite		
1		−11.03	−4.51	
2		−13.41	−2.95	
3		−16.07	−1.85	
		Canada glendonite		
1		−17.23	−6.86	
2		−17.61	−5.83	
3		−18.42	−5.04	

The depth below seafloor at which the ikaite precipitation was initiated and proceeded is difficult to establish. This is partly because the carbon isotope effect between $\delta^{13}C_{DIC}$ and $\delta^{13}C_{ikaite}$ associated with ikaite formation is poorly known. Some authors [77–79] have suggested that the carbon isotope fractionation for ikaite-DIC ($\alpha C_{ikaite\text{-}DIC}$) is small in the range of $\alpha C_{ikaite\text{-}DIC}$ = 1.0006 to 1.003. The $\alpha C_{ikaite\text{-}DIC}$ could be calculated directly from our isotope measurements, **provided** that the crystal is in equilibrium with the current interstitial fluid bicarbonate pool. At the present depth of ikaite occurrence (714–727 cm bsf), the $\delta^{13}C_{DIC}$ is ca. −12.8‰. Using the $\overline{\delta^{13}C_{ikaite}}$ ~ −18‰ for the outer crystal surface, then, according to Equation (2), $\alpha C_{ikaite\text{-}DIC}$ would be approximately 0.995, i.e., the ikaite is ^{12}C-depleted relative to the interstitial fluid DIC. This carbon isotope partitioning would indicate a reverse isotope effect, i.e., the solute phase is enriched in the heavier isotope relative to the mineral phase—a highly unlikely situation.

The formation of other hydrated carbonate minerals, for example, gaylussite ($Na_2CO_3 \cdot CaCO_3 \cdot 5H_2O$) or trona ($Na_2CO_2 \cdot NaHCO_3 \cdot 5H_2O$), reported by [80], have carbon isotope fractionation factors estimated at −1.4 °C to be $\alpha C_{gaylussite\text{-}DIC}$ = 1.0035 and $\alpha C_{trona\text{-}DIC}$ = 1.002, respectively. For comparison, based on the work of [81], the fractionation $\alpha C_{calcite\text{-}DIC}$ would be 1.0011 at −1.4 °C. The revision by [82] would set $\alpha C_{calcite\text{-}DIC}$ = 0.9995 at −1.4 °C. Unfortunately, there is less information available on the isotope fractionation for other hydrated carbonate minerals, such as nahcolite ($NaHCO_3$) or eitelite ($Na_2Mg(CO_3)$ found in alkaline lakes [83], for comparative purposes.

These estimates of the ikaite-DIC carbon fractionation do not take into account rates of crystallization, which, as pointed out by [84], can lead to kinetic isotope effects at high precipitation rates, potentially decreasing the overall carbon isotope fractionation.

Similar to ikaite, the transformation process of vaterite to calcite or aragonite and possibly amorphous calcium carbonate, is potentially inhibited in the presence of phosphate [85] and stabilized by sulfate [86]. Furthermore, the vaterite can be more enriched in ^{13}C by freezing and rapid growth rates [87,88].

Accordingly, we propose that the ikaite surface is not in equilibrium with the current interstitial DIC at 714–727 cm bsf where it is recovered; therefore, the calculated $\alpha C_{ikaite\text{-}DIC}$ of 0.995 is incorrect. Rather, the ikaite formed at an earlier stage, when it was situated

shallower in the sediment column at lower $\delta^{13}C_{DIC}$, likely in the methanogenic zone, beneath the sulfate-reduction/anaerobic methane oxidation zone.

Applying a more reasonable range for $\alpha C_{ikaite\text{-}DIC}$ to be between 1.001 and 1.003, and assuming equilibrium, then the current ikaite surface with $\delta^{13}C_{ikaite} = -17.5‰$ was formed in the sediment where the $\delta^{13}C_{DIC}$ of the interstitial fluid bicarbonate was between −18.5 and −20.4‰. Correspondingly, the interior of the ikaite crystal ($\delta^{13}C_{ikaite} = -21.4‰$) would have formed from the interstitial fluid bicarbonate with a $\delta^{13}C_{DIC}$ between −22.4 and −24.3‰, depending on the chosen $\alpha C_{ikaite\text{-}DIC}$. This indicates that the $\delta^{13}C_{DIC}$ of the bicarbonate from which the ikaite was formed was about 10‰ enriched in ^{12}C compared with the bicarbonate $\delta^{13}C_{DIC}$ at the present depth of ikaite occurrence (727 cm bsf). Choosing a median $\alpha C_{ikaite\text{-}DIC}$ value of 1.002 and using the surface and interior $\delta^{13}C_{ikaite}$ values of −17.5‰ and −21.4‰, respectively, gives a range in $\delta^{13}C_{DIC}$ from −19.5‰ to −23.4‰. This implies that the ikaite single crystal grew while it was situated between 330 and 400 cm bsf (Figure 6, right panel). It is notable that the depth of 330 cm bsf corresponds to just beneath the base of the SRZ and methane oxidation zones. This assumes, of course, that the present interstitial fluid profiles have remained constant, i.e., in steady state, over the last few thousand years. Ikaite formation at the base of the SRZ has also been reported by others [89]. As the ikaite crystal grew between 320 and 385 cm bsf, it remained in contact with the interstitial fluid bicarbonate pool. The $\delta^{13}C_{DIC}$ of this pool was being progressively enriched in ^{13}C due to the faster removal of light bicarbonate (^{12}C) by the methanogens. This led to the pronounced carbon isotope zonation profile measured across the crystal growth structure (Figure 7). Once the crystal growth ceased near the base of the sulfate zone (ca. 385 cm bsf), the interstitial $\delta^{13}C_{DIC}$ continued to be depleted in ^{12}C due to carbon isotope fractionation during methanogenesis until the carbon isotope separation between the crystal surface and the DIC became the 5.6‰ that is measured now. As mentioned above, the postulate that the current crystal surface is in equilibrium with the DIC at 720 cm bsf could only be tenable if the fractionation factor $\alpha C_{ikaite\text{-}DIC}$ would be 0.994, which is the opposite of the isotope effect expected for carbonate mineral precipitation in hydrated and anhydrous phases.

4.4. Oxygen Isotope Zonation

The stable O-isotopes of the interstitial water in core ANT 1138-4 remain constant with sediment depth of $\delta^{18}O_{H2O}$ around $-0.1 \pm 0.1‰$ (Figure 2, Table 1). This is consistent with values for Antarctic bottom waters ($\delta^{18}O_{H2O}$ of −0.29‰, VSMOW) [90]. The uniformity of $\delta^{18}O_{H2O}$ with sediment depth indicates either that the bottom water incorporated into the sediments has not changed significantly over the time spanned by the core, as supported by the ^{14}C radiometric dates, or that vertical fluid movement has exchanged and homogenized the interstitial water. The latter is unlikely, in consideration of the dissolved nutrient and $\delta^{13}C_{DIC}$ profiles, which most certainly would also have uniform distributions resulting from diffusive mixing.

The cross-sectional profile of the carbonate oxygen isotope ratios in ikaite crystal K735 ($\delta^{18}O_{ikaite}$) systematically change along the 16 mm cross section sample traverse (Figure 7), analogous to that observed for $\delta^{13}C_{ikaite}$. The three surface samples along the length of the crystal (numbers 1, 2, and 3 in Figure 7) have a consistent $\delta^{18}O_{ikaite}$ values of +1.58, +1.46, and +1.60‰, respectively. The outermost (younger) samples in the cross section (numbers 4 and 10), with $\delta^{18}O_{ikaite}$ values of +2.32 and +1.67‰, respectively, are similar to the surface $\delta^{18}O_{ikaite}$ values. However, these samples are significantly depleted in ^{18}O, in comparison with the innermost (older) section (sample 7), which has a $\delta^{18}O_{ikaite}$ of +4.5‰. Relative to the interstitial water, the oxygen isotope fractionation between carbonate ikaite and water ranges from $\alpha O_{ikaite\text{-}H2O}$ of 1.0046 (innermost, sample 7) to 1.0016 (outermost, sample 4).

The oxygen isotope separation between the ikaite carbonate and the formation water can potentially provide information on the processes of precipitation, recrystallization, and formation temperature. However, the determination of formation temperature is complicated by several factors, including lack of equilibrium and the possible partitioning

of oxygen between the carbonate oxygen ($\delta^{18}O_{ikaite}$) and the contamination (mixing and/or exchange) by the hydration water oxygen. In addition, the magnitude of the isotope fractionation between ikaite and the interstitial water ($\alpha O_{ikaite\text{-}H2O}$) may also be controlled by factors which include the degree of Ca, DIC saturation, and rate of formation [91]. Furthermore, it is clear that the simple application of Equations (2) and (12) to estimate temperatures of hydrated or cryogenic carbonates, such as ikaite, monohydrocalcite, or calcium carbonate hemihydrate, may not be valid. Recognizing the limitations, the standard ^{18}O-paleotemperature expression for the equilibrium precipitation of calcite from seawater (e.g., as in [92], based on [93,94]) can be very tentatively used to compare the calculated vs. actual temperature of the ikaite formation, i.e.,

$$T\ (^{\circ}C) = 15.7 - 4.36\left(\delta^{18}O_{calcite} - \delta^{18}O_{water}\right) + 0.12\left(\delta^{18}O_{calcite} - \delta^{18}O_{water}\right)^2, \quad (12)$$

where $\delta^{18}O_{calcite}$ is relative to VPDB and $\delta^{18}O_{water}$ is relative to VSMOW. Recognizing these cautions and constraints, the corresponding ikaite formation temperature calculation using Equation (12) gives a range in the formation temperature, from −1.7 °C for the innermost (oldest) part to 9.2 °C for the surface (youngest) of the crystal (Figure 7, Table 2). The warmest values are clearly unreasonable, considering the known sediment temperatures in the Bransfield Strait. Furthermore, it is unlikely that the shift is due to a restricted interstitial water reservoir that became enriched in ^{18}O with time, nor the interstitial water of the sediment column exchanging completely over time and with a varying $\delta^{18}O_{H2O}$. The change in $\delta^{18}O_{ikaite}$ across the crystal also cannot be explained by partial recrystallization of ikaite to calcite because microscopic, X-ray diffraction (XRD) and crystallographic measurements have confirmed that the recovered crystals are entirely intact ikaite [47].

The precipitation of ikaite is associated with an oxygen isotope fractionation of the carbonate oxygen that is lower than that of calcite, as represented by the outer, most recent section of the crystal ($\alpha O_{ikaite\text{-}H2O}$ = 1.0016). Rickaby et al. (2006) [95] determined experimentally over a $\delta^{18}O_{water}$ range from −3.6 to 17.9‰ SMOW, that the oxygen isotope fractionation between the ikaite hydration water $\delta^{18}O_{hydration}$ and $\delta^{18}O_{water}$ was constant at ~−2.9‰ (2 °C), i.e., an $\alpha O_{hydration\text{-}water}$ of 1.0029. In contrast, and curiously, the carbonate $\delta^{18}O_{ikaite}$ in the Rickaby et al. (2006) [95] experiments did not vary with $\delta^{18}O_{water}$ and was constant at ~11‰. This calculates as an $\alpha O_{ikaite\text{-}H2O}$ of 0.9619 to 0.9812 compared with the $\alpha O_{ikaite\text{-}H2O}$ of 1.0046 to 1.0016 for our Bransfield Strait ikaite. Studies of vaterite (μ-$CaCO_3$), a metastable polymorph of calcium carbonate formed via dehydration [96], exhibit oxygen isotope fractionation of an $\alpha O_{vaterite\text{-}H2O}$ similar to calcite, i.e., ~1.028 at 25 °C [97–99]. Grasby (2003) [88] found an $\alpha O_{vaterite\text{-}H2O}$ of ~ 1.035, similar to $\alpha O_{calcite\text{-}H2O}$ at 2 °C. Some support for this is suggested from the isotope fractionation of mirabilite ($Na_2SO_4{\cdot}10H_2O$), which has an $\alpha O_{mirabilite\text{-}H2O}$ of 1.0020 at 0 °C [100] and for gypsum ($CaSO_4{\cdot}2H_2O$) an $\alpha O_{gypsum\text{-}H2O}$ of 1.003–1.0041 [101,102].

Although there is evidence that the ikaite crystal was intact prior to sampling, we cannot fully eliminate the possibility that the metastable ikaite crystal had slowly decomposed in situ to vaterite, aragonite, calcite, or amorphous calcium carbonate and H_2O. In this case, the ikaite crystal initially may have had a uniform $\delta^{18}O_{ikaite}$ distribution of around +1.5‰, but potential recrystallization to vaterite/calcite proceeds gradually outward from the older, center of the ikaite crystal. Re-establishment of the oxygen isotope equilibrium for the newly formed calcite near the center of the crystal, with respect to the sediment temperature of −1.4 °C, would predict an oxygen isotope fractionation between the ikaite calcite and interstitial water of 5.2‰, which is comparable to the measured 4.5‰. Recrystallization would not affect the distribution of carbon isotopes in the ikaite zonal structure owing to slow carbon exchange rates, carbon reservoir size, and conservative transfer.

4.5. Hydrogen Isotopes in Ikaite Hydration Water

Similar to the oxygen isotopes, the stable hydrogen isotopes of the interstitial water in core ANT 1138-4 remained constant, with sediment depth with a δ^2H_{H2O} around

-5.7 ± 0.9‰ (Figure 2, Table 1) and were consistent with the values for Antarctic bottom waters (δ^2H_{H2O} of -3.3‰, VSMOW) [90]. Hydrogen isotope measurements of the ikaite crystal water were made only on bulk samples of the mineral. From a total of five measurements on two samples, the bulk hydrogen isotope ratio for the crystal water (δ^2H_{ikaite}) was around -14.4 ± 2.9‰ (VSMOW). The technique employed here could not isolate the possible influences of inclusion water, disequilibrium growth, or postformation exchange effects on the $^2H/^1H$ of the crystal water. The corresponding measurements of $\delta^{13}C_{DIC} = -17.5$‰ and $\delta^{18}O_{ikaite} = +1.4$‰ (VPDB) indicate that the bulk sample was from the outer portion of the hydrate, as noted earlier (Section 4.3). Relative to the present isotope ratios of the interstitial water in the core, the bulk ikaite sample was depleted in deuterium by 11‰, i.e., the hydrogen fractionation factor between the crystal-hydrate H_2O (ikaite) and the interstitial water (H_2O) was $\alpha H_{ikaite\text{-}H2O} = 0.989$. Although the hydrogen isotope effects associated with the formation of ikaite are unknown, the depletion of deuterium in the hydrate crystal water over that of the interstitial water is in excellent agreement with those typically observed for several other hydrated minerals. A deuterium depletion in the crystal H_2O of various salts relative to the solution H_2O, e.g., $\alpha H_{CuSO4\text{-}H2O} = 0.978$ (25 °C), was reported by [103]. Hydrogen fractionation for gypsum was found by [104] to be constant with the temperature: $\alpha H_{gypsum\text{-}H2O} = 0.985$ between 17 and 57 °C. Also comparable with ikaite is gaylussite ($Na_2CO_3{\cdot}CaCO_3{\cdot}5H_2O$), a similar hydrated carbonate discussed above with respect to its carbon isotope fractionation, having $\alpha H_{gaylussite\text{-}H2O} = 0.987$ at 18 °C [80]. However, the latter authors reported larger fractionations for nahcolite (estimated 20 to 90‰ depletion) and trona (calculated at −1.4 °C as a 110‰ depletion), while borax formed essentially without fractionation. In contrast to the trend observed for ikaite and other hydrates, deuterium was found to be enriched in mirabilite ($Na_2SO_4{\cdot}10H_2O$) relative to the formation solution, $\alpha H_{mirabilite\text{-}H2O} = 1.019$ [100].

5. Implications of Ikaite Occurrences

5.1. Formation Conditions and Cold Temperature Recorders

Calcium carbonate pseudomorphs, commonly referred to as thinolites, glendonites, or gennoishi, etc., have been described worldwide from environments comparable to the Bransfield Strait basin, but also from Pleistocene glacial lakes, deep-sea trenches, and pre-Cambrian continental shelves and shelf basins (for reviews see: [44–46,105–108]). Their pseudomorph crystal form and frequent association with organic-rich and phosphorite-containing sediments in colder or polar environments provide evidence that these carbonates are relics of recrystallized ikaites [106]. Although often speculated to be an indicator of colder paleoenvironments, ikaite pseudomorphs are not necessarily unique to such conditions. As noted earlier, [20,21] demonstrated the metastable character of ikaites and these minerals have been reported from various sedimentary environments regardless of temperature, notably the Nankai Trough [7].

The chemical literature of the l9th and early 20th century abounds with reports on hydrated $CaCO_3$ phases, the calcite hexahydrate being the one most commonly synthesized by artificial nucleation [3–5,109]. The precipitation of ikaite in preference over calcite or aragonite is not exclusively temperature-controlled, rather it was suspected that the presence of inorganic and/or organic crystallization nuclei or inhibitors may determine which carbonate phase is formed. Additives such as sucrose, protein, mollusk and arthropod blood, and polyphosphates, but also Mg, Co, and Ni, were all observed to favor hexahydrate precipitation over that of anhydrous calcium carbonate at low temperatures [2,110,111].

Early studies indicated that $CaCO_3{\cdot}6H_2O$ precipitation could also be induced without additives at subzero temperatures, under carefully chosen conditions of maintaining supersaturation [18]. Works by [20,21] showed that $CaCO_3{\cdot}6H_2O$ is a phase more stable than aragonite and calcite at high water pressures of up to 6 kbars at 25 °C. Experimental studies thus indicate that the formation of calcium carbonate hexahydrate is strongly favored by low temperatures, and that increased water pressure or certain additives, which do not necessarily enter into the crystal lattice, or both, could lead to metastable precipitation

at appreciably higher temperatures. We think that herein lies an explanation for their formation in disparate temperature regimes.

Natural, sedimentary ikaite is known to occur as metastable species within the approximate temperature range from −2 to +7 °C [106]. Experimentally, ikaite has been formed at higher temperatures up to 12 °C [112] and even 35 °C [22,113,114], with and without high pH, salinity, alkalinity, and inorganic precipitation additives, such as phosphate or magnesium [9,16,115–118]. Generally, however, these crystals quickly decompose to vaterite, aragonite, and calcite [16,19,22,119–121].

It is well understood that orthophosphate, and in particular $CaPO_4$ and $CaHPO_4^o$, can inhibit calcite precipitation and thereby promote ikaite formation [19,122–126]. Phosphate concentrations in the Bransfield Strait interstitial fluids are up to 0.54 mM (Table 1), which is 100–500 times greater than the typical 1–4 µM in seawater. The threshold for phosphate inhibition of calcite formation was reported by [125–127] to be ~5 µM, i.e., ~100 times lower than the interstitial fluids around the SRZ (Figure 4). In contrast, experiments demonstrated that phosphate was not important for the precipitation of ikaite in Ikka Fjørd [114] or sea ice [116,120]; rather, it is the high degree of carbonate supersaturation, pH, and potentially being coupled with Mg inhibition. Interestingly, the authors of [114] also noted that hydrated Mg carbonates, i.e., lansfordite ($MgCO_3 \cdot 5(H_2O)$) and nesquehonite ($MgCO_3 \cdot 3(H_2O)$), may coprecipitate with ikaite.

Calcium and magnesium in the Bransfield Strait interstitial fluids range from 5.7 to 10.5 mM and from 49.6 to 53.8 mM, respectively (Table 1), which is similar to the present-day mean ocean water values (Ca 10.3 mM and Mg 53 mM [128]). Experiments by [22] at 5 °C, using a pH range of 9–10.5, and sodium ratios have shown that ikaite is formed at Mg concentrations above ~5 mM, i.e., 10 times lower than present in the interstitial fluids. Similarly, experiments by [23] showed a significant suppression of calcite formation at Mg > 5 mM. They also demonstrated that $MgSO_4$ and SO_4 (also in combination with Mg) substantially inhibited calcite at concentrations of ~3 mM and 10 mM, respectively. In contrast, [129] reported that the highest Mg:Ca is associated with the least-stable ikaite and the Mg may, in fact, destabilize ikaite. The molar Mg:Ca may also be an important factor for calcite inhibition and therefore promotion of ikaite formation [112]. The Bransfield Strait interstitial fluid Mg:Ca (molar) varies from 4.8 to 7.2 in the interstitial fluids (Table 1) and is similar to modern seawater with a mean Mg:Ca of 5.1 [130] and range of 4.5 to 6.5 [128].

The inhibition of calcite formation by sulfate has been proposed by several studies [22,23]. Considering that the ikaite in the Bransfield Strait forms at the base of the SRZ, which was also observed by [89], it may perhaps suggest that all carbonate formation, not just calcite, is suppressed in the SRZ. However, although it seems to contradict the support from several studies which have concluded that ikaite forms in the presence of sulfate [131], there is evidence that sulfate can enhance the inhibition effects of Mg [15,23,125,127].

Although we cannot fully resolve the parameters critical for ikaite formation in this paper, it is noteworthy that the ikaite formed in the Bransfield Strait sediments is at the depth where the phosphate concentration is at a maximum, Mg is at a minimum, and is directly beneath the transition zone of sulfate-reduction/anaerobic methane oxidation and methanogenesis (Figure 2).

5.2. Amino Acids

In addition to inorganic inhibitors, we suggest that naturally occurring organic compounds, characteristically enriched in acidic amino acids and other nonprotein amino acids, could favor the formation of ikaites in environments such as the Bransfield Strait basin.

This effect is clearly evident in the amino acid spectrum of the hydrolysable organic residue isolated from ikaite crystals (Table 3, Figure 8). Its outstanding feature is the dominance of aspartic acid, glutamic acid, and glycine. Together, they constitute more than 50 mol %. If we include beta-alanine, which is considered a degradation product of aspartic acid, then they account for more than 60% of all amino acids. Such dominance is diagnostic for the composition of biogenic carbonate-secreting tissues as well

as for selectively sorbed organics thought to constitute organic templates, which induce inorganic calcite precipitation from seawater [132,133]. The potential influence of cold-active/alkaline-active enzymes, such as phosphatase, α-galactosidase, protease, α-amylase, β-galactosidase, and β-glucanase, on ikaite formation is also uncertain, but they have been found together [134–136]. In addition, certain rare amino acids from bacterial metabolism (alpha-AAA, alpha-APA, and gamma-ABA) were also present in significant quantities in the ikaite residue. It is likely that they originate from the methanogenic microbial population present in the Bransfield Strait sediments. The presence of these amino acids may eventually constitute a tracer for this particular diagenetic environment. Peculiar to the Bransfield Strait are the relatively high amounts of serine and threonine, two amino acids known to be concentrated in biogenic silica-secreting tissues. These are not unexpected in the diatom-rich plankton and sediments of the high latitudes. We are uncertain at this stage if any diagnostic amino acids are preserved in ancient pseudomorphs or glendonites. It certainly would be a worthwhile project to search for such organic tracers in ancient ikaites/glendonites.

Table 3. Amino acids of hydrolysable residue from ikaite crystals, plankton, and sediments from the Bransfield Strait, Antarctica. Concentrations in μg/g.

Amino	Plankton	Sediment	Ikaite
acid	residues/1000		
cyst	3	3	94 **
tau *	1	1	28 **
meto	3	3	40 **
asp	108	142	209 ****
thr″	57	62	42
ser″	75	87	72
glu	101	79	61 ****
alpha-AAA	<1	< 1	8
gly	87	212	242 ****
ala	106	93	44
val	71	52	29
met	13	9	6
alpha-APA	<1	< 1	3 ***
allo-ileu	<l	1	1
ileu	56	33	11
leu	105	47	10
tyr	28	15	3
phe	53	27	8
beta-ala	3	10	77 *,**
gamma-ABA	<1	4	7 **
orn	<l	5	8 **
lys	70	60	64
his	15	13	9
arg	45	44	4

Concentrations in μg/g; * complex mixture with taurine; ** degradation products: beta-ala from aspartic acid taurine, cysteic acid from cysteine and methionine, gamma-ABA from glutamic acid, ornithine from arginine, and/or bacterial biomass: alpha-DPA and alpha-AAA; *** beta-ala: here very likely from degradation of aspartic acid; **** amino acids in Ca-carbonate-secreting organic templates; amino acids of silica-secreting tissue concentrated in Bransfield Strait plankton.

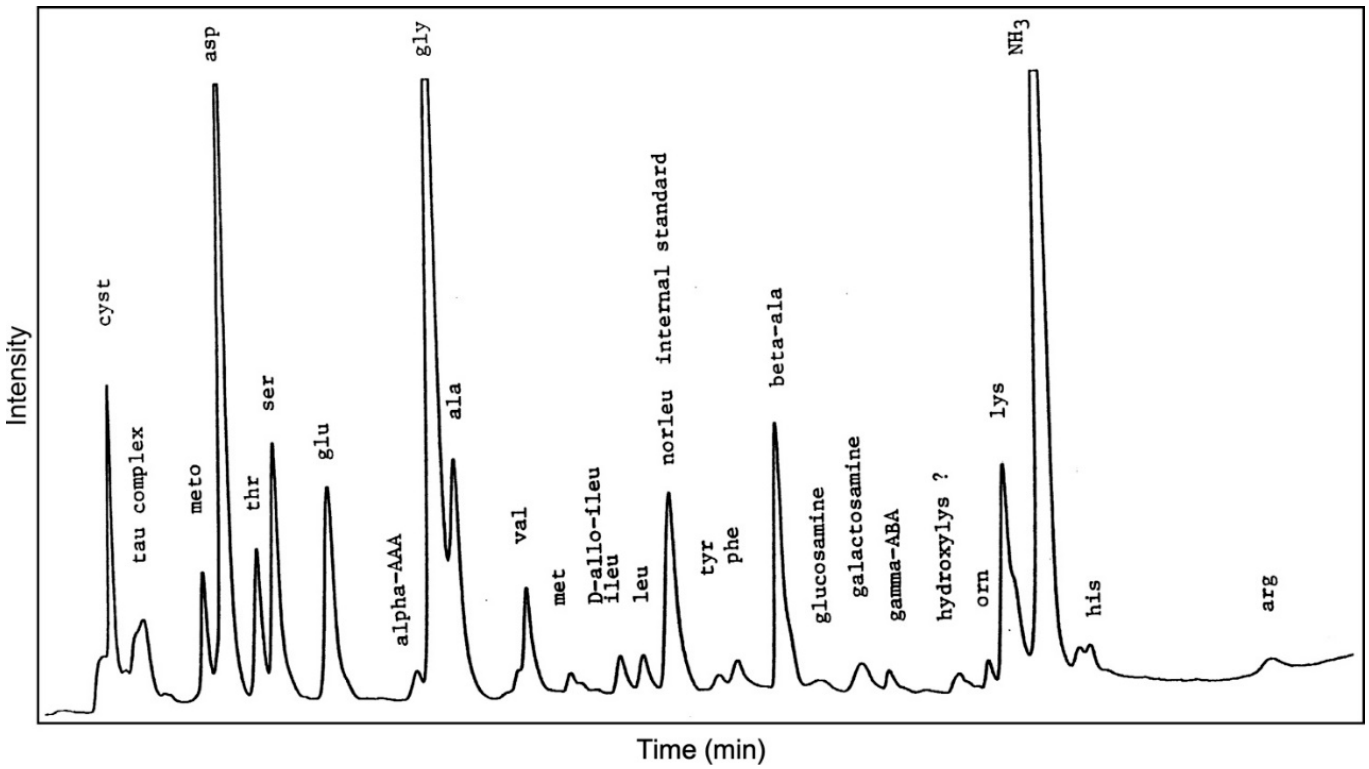

Figure 8. Amino acid chromatogram from hydrolysable organic matter for the insoluble residue from the Bransfield Strait ikaite. Norleucine (indicated) was used as internal standard. The dominance of aspartic acid and beta-alanine, the degradation product of aspartic acid, are the dominant species measured. Aspartic acid may potentially induce the metastable formation of ikaite compared with calcite or aragonite.

5.3. Glendonites

In an initial attempt to trace to ancient environments, the isotope signal established during the formation of ikaite, and its subsequent recrystallization, we profiled two samples of calcite pseudomorphs (glendonites from Spitzbergen and Canada) for $\delta^{13}C_{glendonite}$ and $\delta^{18}O_{glendonite}$. The carbon isotope profiles across the two pseudomorphs show that the $\delta^{13}C_{glendonite}$ became progressively ^{13}C-depleted, moving from the inside to the outside of the sample (Figure 9, Table 2). The $\delta^{18}O_{glendonite}$ of the two samples became enriched in ^{18}O from inside to outside. Although the magnitude of the C- and O-isotope shift in the glendonites is similar to that of the Bransfield Strait ikaite, the values of $\delta^{13}C$ and $\delta^{138}O$ differ. In particular, the ikaite became ^{13}C-enriched, moving from inside to outside. Analogously, Rogov et al. (2017) [137] showed profiles across glendonites with $\delta^{13}C_{glendonite}$ from ~−21 to −17‰ and $\delta^{18}O_{glendonite}$ ranging from ~−3 to −12‰ in response to changing diagenetic fluids. Wang et al. (2020) [46] reported spot analyses of four individual glendonites. Samples from the interior to exterior had $\delta^{13}C_{glendonite}$ changing from −27.9‰ to −1.7‰ and $\delta^{138}O_{glendonite}$ from −9.4‰ to −12.5‰.

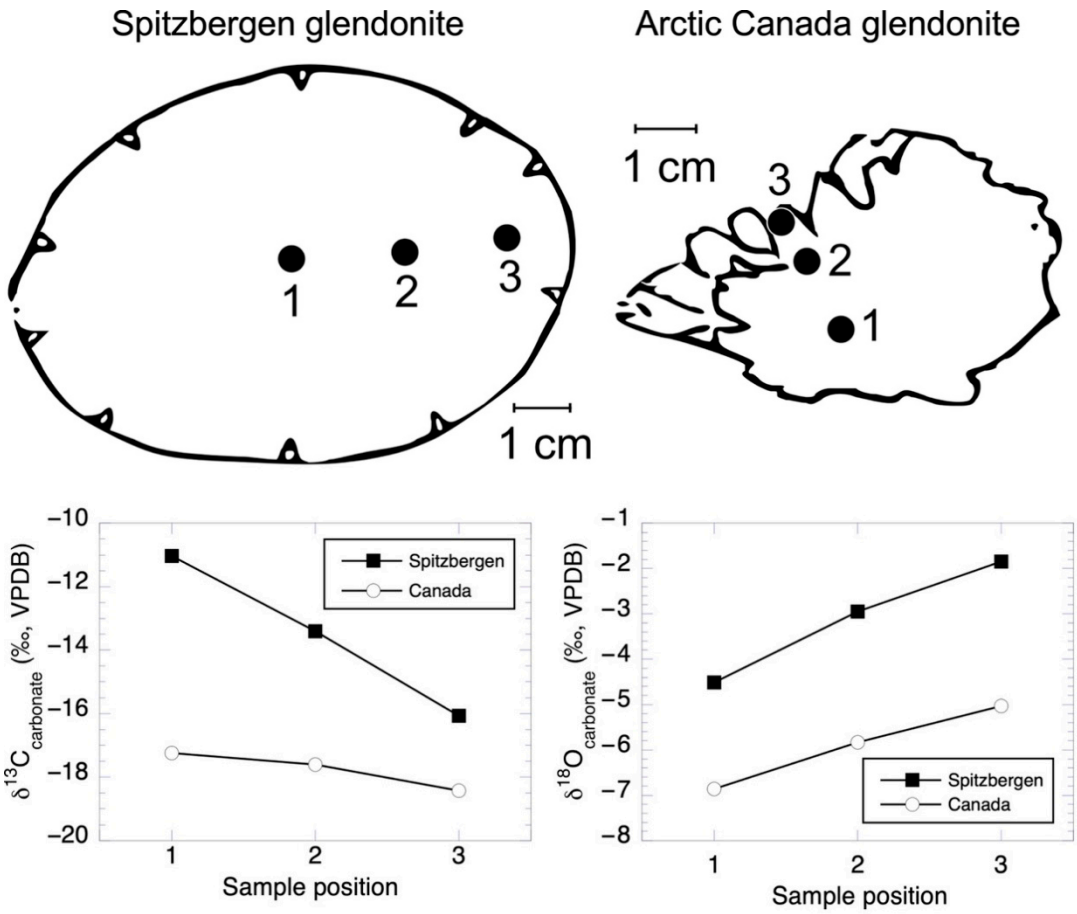

Figure 9. Carbon and oxygen isotope measurement traverse across glendonite pseudomorphs of ikaite from Spitzbergen and Canada. Changes in $\delta^{13}C_{glendonite}$ likely reflect diagenetic changes in $\delta^{13}C_{DIC}$ of the DIC pool during growth of original ikaite. The changes in $\delta^{18}O_{glendonite}$ are possible due to kinetic isotope effects during transformation or resetting of oxygen isotope composition during recrystallization of ikaite to calcite.

The $\delta^{13}C_{carbonate}$ and $\delta^{18}O_{carbonate}$ for ikaites and glendonites worldwide of the Phanerozoic age have been compiled by [46,138]. The isotopes measured in these papers are measured on bulk, spatially undifferentiated samples, i.e., not profiles of crystals or pseudomorphs. Thus, they may not be directly comparable to the more systematic inter-glendonite transects we report here. Figure 10 shows the very wide spread in isotope values for ikaites and glendonites with $\delta^{13}C_{carbonate}$ ranging from −45 to +5.8‰ and $\delta^{18}O_{carbonate}$ ranging from −17 to +0.3‰ (Table 4). The most ^{12}C-depleted glendonites (−30 to −45‰) are clearly strongly influenced by DIC derived from methane oxidation and have invariant $\delta^{18}O_{carbonate}$ of around 0 to −5‰. Otherwise, in Figure 10, to a first approximation, as the ikaite and glendonite $\delta^{13}C_{carbonate}$ values become more ^{13}C enriched, they are accompanied by $\delta^{18}O_{carbonate}$ depleted in ^{18}O. Although both the $\delta^{13}C_{carbonate}$ and $\delta^{18}O_{carbonate}$ are responding to changing diagenetic fluid isotope compositions and environmental conditions, e.g., temperature, the explanation for this trend is not immediately apparent. It is unclear whether this glendonite $\delta^{13}C_{carbonate}$–$\delta^{18}O_{carbonate}$ behavior is coincidental or whether there is a causal, sympathetic mechanism that systematically enriches/depletes the carbonate ^{18}O and ^{12}C. Similar trends have been reported for glendonites in Siberia [139]. We suspect that these trends are controlled more by the environmental conditions under which the ikaite structure changes to calcite. Specifically, the trend in oxygen isotopes would be reversed if such recrystallization occurred under higher or lower temperatures than that at which the initial ikaite formed. The carbon and oxygen isotopes would respond if the change was

accompanied by a drastic change in fluid chemistry, such as from meteoric waters or fluids charged with different partial pressures of DIC.

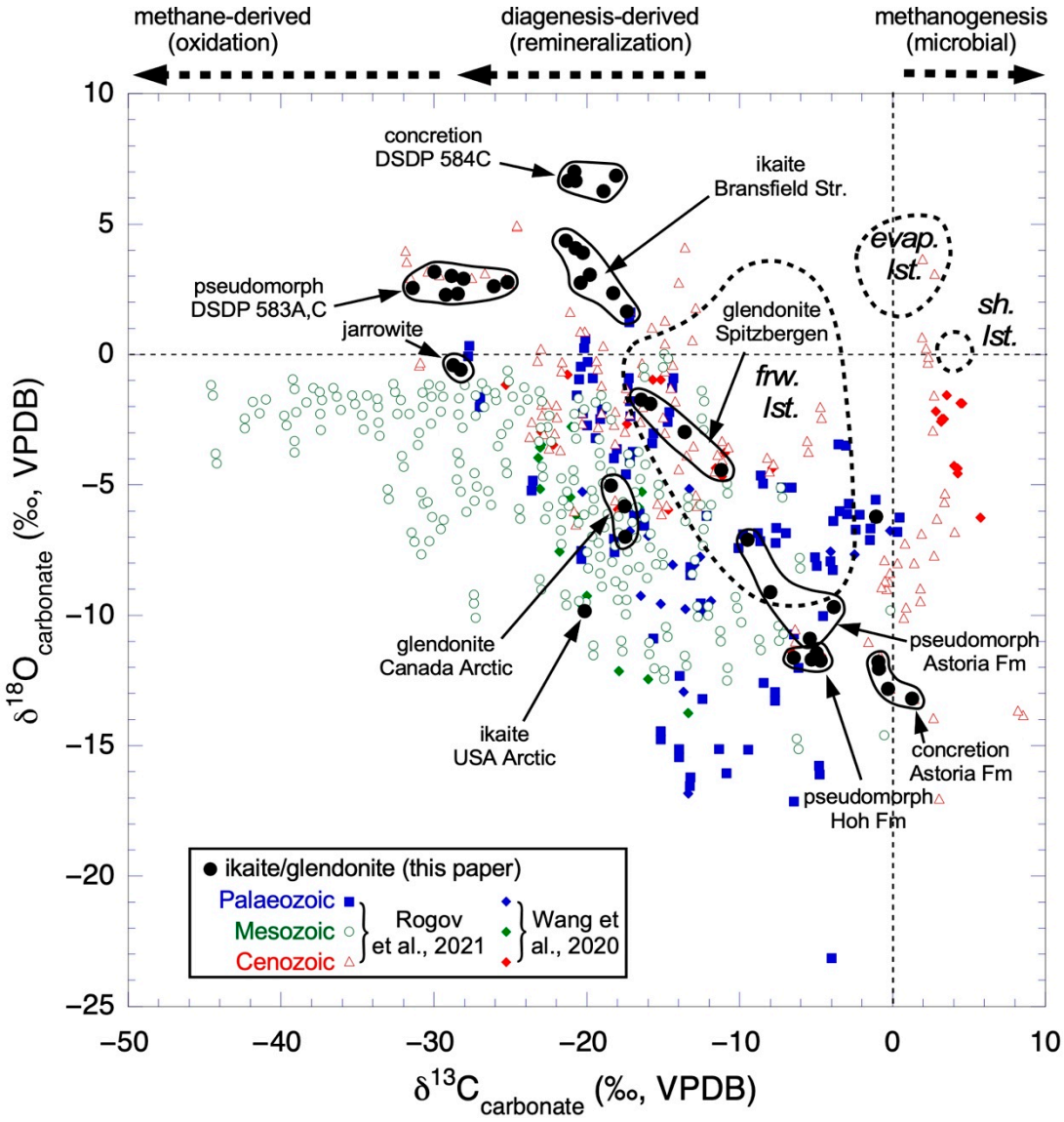

Figure 10. Plot of $\delta^{18}O_{carbonate}$ vs. $\delta^{13}C_{carbonate}$ for ikaite and glendonite samples reported in this paper. For reference the Phanerozoic (Paleozoic, Mesozoic, and Cenozoic) $\delta^{18}O_{glendonite}$ vs. $\delta^{13}C_{glendonite}$ databases of Rogov et al. (2021) [138] and Wang et al. (2020) [46] are shown. The wide range in isotope values largely reflects the differences in diagenetic settings and processes, rather than temperatures.

Table 4. Maximum and minimum carbon and oxygen isotope ratio values of glendonites in databases from Rogov et al. [138] and Wang et al. [46].

	$\delta^{13}C_{carbonate}$ (‰, VPDB)		$\delta^{18}O_{carbonate}$ (‰, VPDB)	
	Minimum	**Maximum**	**Minimum**	**Maximum**
	Rogov et al., 2021 [138]			
Paleozoic	−27.7	0.4	−23.3	1.6
Mesozoic	−44.6	−0.1	−15.1	0.0
Cenozoic	−31.9	8.5	−17.0	4.9
	Wang et al., 2021 [46]			
Paleozoic	−27.7	0.6	−16.9	0.3
Mesozoic	−45.2	0.0	−14.7	0.0
Cenozoic	−25.2	5.8	−11.6	−0.8

As in the case of ikaite formation and decomposition, kinetics can substantially influence the isotope composition [91,102,140–142]. The comprehensive Phanerozoic glendonite databases from [46,138] clearly show the wide range in $\delta^{13}C_{glendonite}$ (~−45 to +8.5‰) and $\delta^{18}O_{glendonite}$ (~23 to +5‰) (Table 4) that also encompass our ikaite and glendonite results, but not our more recent ones reported elsewhere [46] (Figure 10). In addition, [107] generated a very similar $\delta^{18}O_{carbonate}$ vs. $\delta^{13}C_{carbonate}$ plot, largely using the same ikaite and glendonite data as in Figure 10. At this point, it is reasonable to make the interpretation that the most strongly ^{13}C-depleted $\delta^{13}C_{glendonite}$ values reflect the ^{12}C-rich DIC derived from the aerobic or anaerobic oxidation of ^{12}C-enriched microbial methane [11,14,139,143,144]. Subsequently, the resultant glendonites are influenced by DIC generated by diagenetic sources. The $\delta^{18}O_{glendonite}$ reflects diagenetic and other alteration influences, but the explanation appears more complicated and calls for further investigations.

There are many indications that low temperatures, such as of a polar environment, climate-related cold spells, high calcium carbonate supersaturation caused by interstitial methanogenesis, and a sufficiently large supply of dissolved organics containing acidic amino acids, favor metastable ikaite formation. Under these conditions we speculate that there might be a partial trade-off, such that an insufficient supply of dissolved organics is compensated for by extremely low temperatures in order for ikaite to form or that higher temperatures may permit ikaite formation only under total pressures of several hundred bars and abundant dissolved organics. The large crystal size and macroscopic dimensions of the pseudomorphs allow a detailed reconstruction of the events of ikaite formation and recrystallization.

There is continued evidence and support that glendonites can serve as cold environmental indicators, such as glaciomarine settings [45,46,95,145–153]. However, there are some concerns that the $\delta^{18}O_{glendonite}$ of glendonites are not robust recorders of low-temperature environments, due to various processes such as dissolution and reprecipitation [129,137,154]. There is also uncertainty with the formation of ikaite and its subsequent conversion to calcite, including possible intermediates and mixtures with monohydrocalcite, vaterite, and aragonite [7,118,155].

It is still a puzzle as to why we only encounter ikaite crystals at ~720 cm bsf, possibly as a "pavement" in the Bransfield Strait. Outstanding questions remain in finding a convincing explanation for why ikaite stops growing in the sediment below ~385 cm bsf and why, in the case of the Bransfield Strait, new ikaite crystals are not continuously and currently forming in shallower portions of the sediment package at the base of the SRZ.

Author Contributions: Conceptualization, E.S., and M.J.W.; methodology, E.S., M.J.W., P.J.M. and G.W.; writing, M.J.W.; funding, E.S. and M.J.W. All authors have read and agreed to the published version of the manuscript.

Funding: This work was supported by the US Office of Naval Research (grant N00014-84-C-0218) and US National Science Foundation (grant DPP-8512395); we also gratefully acknowledge the financial support from the Oregon State University Foundation (E.S.) and the Hanse-Wissenschaftskolleg (M.J.W.).

Acknowledgments: We (M.J.W., E.S., and G.W.) dedicate this paper to our lost, dear friend and colleague, Peter Müller, who was always a great companion in the lab and at sea. We thank the master and crew of the PRSV Polarstern, under the direction of the Alfred Wegener Institute for Polar Research in Bremerhaven, Germany, for their outstanding and highly professional assistance at sea.

Conflicts of Interest: The authors declare no conflict of interest.

References

1. Hume, J.; Topley, B. CCCXC—The density of calcium carbonate hexahydrate. *J. Chem. Soc.* **1929**, *129*, 2932–2934. [CrossRef]
2. Dickens, B.; Brown, W.E. The crystal structure of calcium carbonate hexahydrate at −120°. *Inorg. Chem.* **1970**, *9*, 480–486. [CrossRef]
3. Daniell, J.F. Some facts relating to the formation and decomposition of sugar, and the artificial production of crystallized carbonate of lime. *Annal. Chim.* **1819**, *10*, 219–224.
4. Becquerel, A.C. Du carbonate de chaux cristallise, et de l'action simultanee des matieres sucrees ou mucilagineuses sur quelques oxides metalliques, par l'intermediaire des alcalis et des terres. *Annal. Chim.* **1831**, *47*, 5–20.
5. Pelouze, J. Sur la production artificielle du carbonate de chaux cristallise, et sur deux combinaisons de ce sel avec l'eau. *Annal. Chim.* **1831**, *47*, 301–307.
6. Pauly, H. IKAIT Nyt mineral der danner skaer. In *Naturens Verden*; E. Munksgaards Forlag, 1963; pp. 168–171; 186–192.
7. Stein, C.; Smith, A.J. *Authigenic Carbonate Nodules in the Nankai Trough, Site 583*; Init. Repts. DSDP 87; Kagami, H., Karig, D.E., Coulbourn, W.T., Eds.; U.S. Government Printing Office: Washington, DC, USA, 1986; pp. 659–668.
8. Jansen, J.; Woensdregt, C.F.; Kooistra, M.J.; Van Der Gaast, S.J. Ikaite pseudomorphs in the Zaire deep-sea fan: An intermediate between calcite and porous calcite. *Geology* **1987**, *15*, 245–248. [CrossRef]
9. Buchardt, B.; Seaman, P.; Stockmann, G.; Vous, M.; Wilken, U.; Düwel, L.; Kristiansen, A.; Jenner, C.; Whiticar, M.J.; Kristensen, R.M. Submarine columns of ikaite tufa. *Nature* **1997**, *390*, 129–130. [CrossRef]
10. Suess, E.; Balzer, W.; Hesse, K.-F.; Müller, P.J.; Ungerer, C.A.; Wefer, G. Calcium Carbonate Hexahydrate from Organic-Rich Sediments of the Antarctic Shelf: Precursors of Glendonites. *Science* **1982**, *216*, 1128–1131. [CrossRef]
11. Schubert, C.J.; Nurnberg, D.; Scheele, N.; Pauer, F.; Kriews, M. ^{13}C depletion in ikaite crystals: Evidence for methane release from the Siberian shelves? *Geo-Mar. Lett.* **1997**, *17*, 169–175. [CrossRef]
12. Zabel, M.; Schulz, H.D. Importance of submarine landslides for non-steady state conditions in pore water systems—Lower Zaire (Congo) deep-sea fan. *Mar. Geol.* **2001**, *176*, 87–99. [CrossRef]
13. Hackworth, M. Mud volcanoes, gas hydrates, and carbonate formation at "warm" seeps in the northern Gulf of Mexico. *Geol. Soc. Am.* **2004**, *36*, 193.
14. Greinert, J.; Derkachev, A. Glendonites and methane-derived Mg-calcites in the Sea of Okhotsk, eastern Siberia: Implications of a venting-related ikaite/glendonite formation. *Mar. Geol.* **2004**, *204*, 129–144. [CrossRef]
15. Burton, E.A. Controls on marine carbonate cement mineralogy: Review and reassessment. *Chem. Geol.* **1993**, *105*, 163–179. [CrossRef]
16. Bischoff, J.L.; Fitzpatrick, J.A.; Rosenbauer, R.J. The solubility and stabilization of ikaite ($CaCO_3 \cdot 6H_2O$) from 0 to 25 °C: Environmental and paleoclimatic implications for thinolite tufa. *J. Geol.* **1993**, *101*, 21–33. [CrossRef]
17. Johnston, J.; Merwin, H.E.; Williamson, E.D. The several forms of calcium carbonate. *Am. J. Sci.* **1916**, *41*, 473–513. [CrossRef]
18. Krauss, F.; Schriever, W. Die Hydrate des Calciumcarbonats. *Z. Anorg. Chem.* **1930**, *188*, 259–273. [CrossRef]
19. Brooks, R.; Clark, L.M.; Thurston, E.F. Calcium carbonate and its hydrates. *Philos. Trans. R. Soc. A* **1950**, *243*, 145–167. [CrossRef]
20. Van Valkenburg, A.; Mao, H.K.; Bell, P.M. Ikaite ($CaCO_3 \cdot 6H_2O$), a phase more stable than calcite and aragonite ($CaCO_3$) at high water pressure. *Geophy. Lab. Year Book* **1970**, *70*, 237–238.
21. Marland, G. Stability of calcium carbonate hexahydrate (ikaite). *Geochim. Cosmochim. Acta.* **1975**, *39*, 83–91. [CrossRef]
22. Tollefsen, E.; Stockmann, G.; Skelton, A.; Mörth, C.-M.; Dupraz, C.; Sturkell, E. Chemical controls on ikaite formation. *Miner. Mag.* **2018**, *82*, 1119–1129. [CrossRef]
23. Nielsen, M.R.; Sand, K.K.; Rodriguez-Blanco, J.D.; Bovet, N.; Generosi, J.; Dalby, K.; Stipp, S.L.N. Inhibition of calcite growth: Combined effects of Mg^{2+} and SO_4^{2-}. *Cryst. Growth Des.* **2016**, *16*, 6199–6207. [CrossRef]
24. Bischoff, J.L.; Fyfe, W.S. Catalysis, inhibition, and the calcite-aragonite problem II: The vaterite-aragonite transformation. *Am. Jour. Sci.* **1968**, *266*, 80–90. [CrossRef]
25. Papadimitriou, S.; Kennedy, H.; Kattner, G.; Dieckmann, G.S.; Thomas, D.N. Experimental evidence for carbonate precipitation and CO2 degassing during sea ice formation. *Geochim. Cosmochim. Acta* **2004**, *68*, 1749–1761. [CrossRef]
26. Geilfus, N.-X.; Carnat, G.; Dieckmann, G.S.; Halden, N.; Nehrke, G.; Papakyriakou, T.; Tison, J.-L.; Delille, B. First estimates of the contribution of $CaCO_3$ precipitation to the release of CO_2 to the atmosphere during young sea ice growth. *J. Geophys. Res. Oceans* **2013**, *118*, 244–255. [CrossRef]

27. Rysgaard, S.; Wang, F.; Galley, R.J.; Grimm, R.; Notz, D.; Lemes, M.; Geilfus, N.-X.; Chaulk, A.; Hare, A.A.; Crabeck, O.; et al. Temporal dynamics of ikaite in experimental sea ice. *Cryosphere* **2014**, *8*, 1469–1478. [CrossRef]
28. Hu, Y.-B.; Dieckmann, G.S.; Wolf-Gladrow, D.A.; Nehrke, G. Laboratory study on coprecipitation of phosphate with ikaite in sea ice. *J. Geophys. Res. Oceans* **2014**, *119*, 7007–7015. [CrossRef]
29. Dieckmann, G.S.; Nehrke, G.; Papadimitriou, S.; Göttlicher, J.; Steininger, R.; Kennedy, H.; Wolf-Gladrow, D.; Thomas, D.N. Calcium carbonate as ikaite crystals in Antarctic sea ice. *Geophys. Res. Lett.* **2008**, *35*. [CrossRef]
30. Field, L.P.; Milodowski, A.E.; Shaw, R.P.; Stevens, L.A.; Hall, M.R.; Kilpatrick, A.; Gunn, J.; Kemp, S.J.; Ellis, M.A. Unusual morphologies and the occurrence of pseudomorphs after ikaite ($CaCO_3{\cdot}6H_2O$) in fast growing, hyperalkaline speleothems. *Mineral. Mag.* **2017**, *81*, 565–589. [CrossRef]
31. Oehlrich, M.B.; Sánchez-Pastor, N.; Mayr, C. On the study of natural and synthetic ikaite crystals. *Revista Soc. Esp. Mineral.* **2009**, *11*, 135.
32. Ito, T. Ikaite from cold spring water at Shiowakka, Hokkaido, Japan. *J. Miner. Pet. Econ. Geol.* **1996**, *91*, 209–219. [CrossRef]
33. Boch, R.; Dietzel, M.; Reichl, P.; Leis, A.; Baldermann, A.; Mittermayr, F.; Pölt, P. Rapid ikaite ($CaCO_3{\cdot}6H_2O$) crystallization in a man-made river bed: Hydrogeochemical monitoring of a rarely documented mineral formation. *Appl. Geochem.* **2015**, *63*, 366–379. [CrossRef]
34. Mikkelsen, A.; Andersen, A.B.; Engelsen, S.B.; Hansen, H.C.B.; Larsen, O.; Skibsted, L.H. Presence and dehydration of ikaite, calcium carbonate hexahydrate, in frozen shrimp shell. *J. Agric. Food Chem.* **1999**, *47*, 911–917. [CrossRef] [PubMed]
35. Careche, M.; Herrero, A.M.; Carmona, P. Raman Analysis of white spots appearing in the shell of argentine red shrimp (*pleoticus muelleri*) during frozen storage. *J. Food Sci.* **2002**, *67*, 2892–2895. [CrossRef]
36. Tansman, G.F.; Kindstedt, P.S.; Hughes, J.M. Crystal fingerprinting: Elucidating the crystals of Cheddar, Parmigiano-Reggiano, Gouda, and soft washed-rind cheeses using powder x-ray diffractometry. *Dairy Sci. Technol.* **2015**, *95*, 651–664. [CrossRef] [PubMed]
37. Ohrazda, C.A. Structural study of the occurrence of Ikaite pseudomorphs in Neoproterozoic metalimestones on Islay, Scotland. Bachelor's Thesis, Stockholm University, Stockholm, Sweden, 2017.
38. Dempster, T.; Jess, S.A. Ikaite pseudomorphs in Neoproterozoic Dalradian slates record Earth's coldest metamorphism. *J. Geol. Soc.* **2015**, *172*, 459–464. [CrossRef]
39. Dana, E.S. *A Crystallographic Study of the Thinolite of Lake Lahontan*; U.S. Government Printing Office: Washington, DC, USA, 1884; Volume 6, p. 3. [CrossRef]
40. David, T.W.E.; Taylor, T.G.; Woolnough, W.G.; Foxhall, H.G. Occurrence of the pseudomorph glendonite in New South Wales. *Rec. Geol. Surv. NSW* **1905**, *8*, 161–179.
41. Boggs, S. Petrography and geochemistry of rhombic, calcite pseudomorphs from mid-tertiary mudstones of the pacific northwest, U.S.A. *Sedimentology* **1972**, *19*, 219–235. [CrossRef]
42. Kaplan, M.E. Kal'citovye psovdomorfozy v jurskich i niznemelovych otlozenijach severa vostocnoj Sibiri (calcitic pseudomorphs in Jurassic and Lower Cretaceous deposits from the northern part of eastern Siberia). *Geol. I Geofiz.* **1978**, *12*, 62–70.
43. Kemper, E.; Schmitz, H.H. Glendonite—Indikatoren des polarmarinen Ablagerungsmilieus. *Geol. Rundsch.* **1981**, *70*, 759–773. [CrossRef]
44. Shearman, D.J.; Smith, A.J. Ikaite, the parent mineral of jarrowite-type pseudomorphs. *Proc. Geol. Assoc.* **1985**, *96*, 305–314. [CrossRef]
45. Wang, Z.; Wang, J.; Suess, E.; Wang, G.; Chen, C.; Xiao, S. Silicified glendonites in the Ediacaran Doushantuo Formation (South China) and their potential paleoclimatic implications. *Geology* **2017**, *45*, 115–118. [CrossRef]
46. Wang, Z.; Chen, C.; Wang, J.; Suess, E.; Chen, X.; Wang, G.; Chen, C.; Xiao, S. Wide but not ubiquitous distribution of glendonites in the Doushantuo Formation, South China: Implications for Ediacaran climate. *Precamb. Res.* **2020**, *338*, 105586. [CrossRef]
47. Hesse, K.; Küppers, H.; Suess, E. Refinement of the structure of Ikaite, $CaCO_3{\cdot}6H_2O$. *Z. Für Krist. Cryst. Mater.* **1983**, *163*, 227–232. [CrossRef]
48. Whiticar, M.J.; Suess, E. Hydrothermal hydrocarbon gases in the sediments of the King George Basin, Bransfield Strait, Antarctica. *Appl. Geochem.* **1990**, *5*, 135–147. [CrossRef]
49. Holler, P. Geotechnical properties of Antarctic deep-sea sediments. *Meteor Forsch. Ergebn.* **1985**, *39*, 23–26.
50. Han, M.W. Dynamics and chemistry of pore fluids in marine sediments of different tectonic settings: Oregon subduction zone and Bransfield Strait extensional basin. Ph.D. Thesis, Oregon St. University, Corvallis, OR, USA, 1988; 295p.
51. Barker, P.F.; Dalziel, I.W.D. Progress in geodynamics in the Scotia Arc Region. In *Geodynamics of the Eastern Pacific Region, Caribbean and Scotia Arcs*; U.S. Department of Energy: Washington, DC, USA, 1983; Volume 9, pp. 137–170. [CrossRef]
52. Han, M.W.; Suess, E. Lateral migration of pore fluids through sediments of an active back-arc basin, Bransfield Strait, Antarctica. *Am. Geophy. Union EOS Trans.* **1987**, *68*, 1769.
53. Suess, E.; Fisk, M.; Kadko, D. Thermal interaction between back-arc volcanism and basin sediments in the Bransfield Strait. *Antarc. J. US* **1987**, *22*, 47–49.
54. Hartmann, M.; Moller, P.J.; Suess, E.; Van Der Weijden, C.H. Chemistry of late Quaternary sediments and their interstitial waters from the NW-African continental margin. *Meteor Forsch.-Ergebn.* **1973**, *24*, 1–67.
55. Whiticar, M.J.; Suess, E.; Wehner, H. Thermogenic hydrocarbons in surface sediments of the Bransfield Strait, Antarctic Peninsula. *Nature* **1985**, *314*, 87–90. [CrossRef]

56. Swainson, I.P.; Hammond, R.P. Ikaite, CaCO3·6H2O: Cold comfort for glendonites as paleothermometers. *Am. Mineral.* **2001**, *86*, 1530–1533. [CrossRef]
57. Coleman, D.D.; Risatti, J.; Schoell, M. Fractionation of carbon and hydrogen isotopes by methane-oxidizing bacteria. *Geochim. Et Cosmochim. Acta* **1981**, *45*, 1033–1037. [CrossRef]
58. McCrea, J.M. On the Isotopic Chemistry of Carbonates and a Paleotemperature Scale. *J. Chem. Phys.* **1950**, *18*, 849–857. [CrossRef]
59. Whiticar, M.J.; Eek, M. Challenges of $^{13}C/^{12}C$ measurements by CF-IRMS of biochemical samples at sub-nanomolar levels. In *International Atomic Energy Agency, New Approaches for Stable Isotope Ratio Measurements*; IAEA-TECDOC-1247; IAEA: Vienna, Austria, 2001; pp. 75–95.
60. Müller, P.J.; Suess, E.; Ungerer, A.C. Amino acids and amino sugars of surface particulate and sediment trap material from waters of the Scotia sea. *Deep Sea Res. Part A Oceanogr. Res. Pap.* **1986**, *33*, 819–838. [CrossRef]
61. Roth, M. Fluorescence reaction for amino acids. *Anal. Chem.* **1971**, *43*, 880–882. [CrossRef]
62. Benson, J.R.; Hare, P.E. 8-phthalaldehyde: Fluorogenic detection of primary aurines in the picomole range. *Proc. Natl. Acad. Sci. USA* **1975**, *72*, 619–622. [CrossRef]
63. Müller, P.J. Isoleucine epimarization in Quaternary planktonic foraminifera: Effects of diagenetic hydrolysis, and leaching, and Atlantic-Pacific intercore correlations. *Meteor Forsch. Ergebn.* **1984**, *38*, 25–47.
64. Whiticar, M.J. The Biogeochemical Methane Cycle. In *Hydrocarbons, Oils and Lipids: Diversity, Origin, Chemistry and Fate*; Handbook of Hydrocarbon and Lipid Microbiology; Wilkes, H., Ed.; Springer: Cham, Switzerland, 2020; pp. 669–746. [CrossRef]
65. Whiticar, M.J.; Faber, E. Methane oxidation in marine and limnic sediments and water columns. In *Advances in Organic Geochemistry*; Leythaeuser, D., Rullkötter, J., Eds.; Pergamon Press: New York, NY, USA, 1985; pp. 759–768.
66. Hoffman, P.F.; Kaufman, A.J.; Halverson, G.P.; Schrag, D.P. A Neoproterozoic snowball earth. *Science* **1998**, *281*, 1342–1346. [CrossRef]
67. Claypool, G.E.; Kaplan, I.R. The origin and distribution of methane in marine sediments. In *Natural Gases in Marine Sediments*; Kaplan, I.R., Ed.; Springer: Berlin/Heidelberg, Germany, 1974; pp. 99–139. [CrossRef]
68. Whiticar, M.; Faber, E.; Schoell, M. Biogenic methane formation in marine and freshwater environments: CO_2 reduction vs. acetate fermentation—Isotope evidence. *Geochim. Cosmochim. Acta* **1986**, *50*, 693–709. [CrossRef]
69. Rayleigh, J.W.S. Theoretical considerations respecting the separation of gases by diffusion and similar processes. *Philos. Mag.* **1896**, *42*, 493–593. [CrossRef]
70. Broecker, W.S.; Oversby, V. *Chemical Equilibria in the Earth*; McGraw-Hill: New York, NY, USA, 1971; 318p.
71. Lennie, A.R.; Tang, C.C.; Thompson, S.P. The structure and thermal expansion behaviour of ikaite, $CaCO_3{\cdot}6H_2O$, from T = 114 to T = 293 K. *Miner. Mag.* **2004**, *68*, 135–146. [CrossRef]
72. Kawano, J.; Shimobayashi, N.; Miyake, A.; Kitamura, M. Precipitation diagram of calcium carbonate polymorphs: Its construction and significance. *J. Phys. Condens. Matter* **2009**, *21*, 425102. [CrossRef] [PubMed]
73. Irwin, H.; Curtis, C.; Coleman, M. Isotopic evidence for source of diagenetic carbonates formed during burial of organic-rich sediments. *Nature* **1977**, *269*, 209–213. [CrossRef]
74. Gautier, D.L.; Claypool, G.E. Interpretation of methanogenic biogenesis in ancient sediments by analogy with processes in modern diagenetic environments. *AAPG Memoir* **1984**, *37*, 112–123.
75. Talbot, M.R.; Kelts, K. Primary and diagenetic carbonates in the anoxic sediments of Lake Bosumtwi, Ghana. *Geology* **1986**, *14*, 912. [CrossRef]
76. Reeburgh, W.S.; Heggie, D.T. Microbial methane consumption reactions and their effect on methane distributions in freshwater and marine environments1. *Limnol. Oceanogr.* **1977**, *22*, 1–9. [CrossRef]
77. Mook, W.G. Isotope geochemistry of carbonates in the weathering zone. In *Handbook of Environmental Isotope Geochemistry. V. 2. The Terrestrial Environment, B*; Fritz, P., Fontes, J.-C., Eds.; Elsevier: Amsterdam, The Netherlands, 1986; pp. 239–270.
78. Romanek, C.S.; Grossman, E.L.; Morse, J.W. Carbon isotopic fractionation in synthetic aragonite and calcite: Effects of temperature and precipitation rate. *Geochim. Cosmochim. Acta* **1992**, *56*, 419–430. [CrossRef]
79. Lu, Z.; Rickaby, R.E.; Kennedy, H.; Kennedy, P.; Pancost, R.D.; Shaw, S.; Lennie, A.; Wellner, J.; Anderson, J.B. An ikaite record of late Holocene climate at the Antarctic Peninsula. *Earth Planet. Sci. Lett.* **2012**, *325–326*, 108–115. [CrossRef]
80. Matsuo, S.; Friedman, I.; I Smith, G. Studies of quaternary saline lakes—I. Hydrogen isotope fractionation in saline minerals. *Geochim. Cosmochim. Acta* **1972**, *36*, 427–435. [CrossRef]
81. Emrich, K.; Ehhalt, D.H.; Vogel, J.C. Carbon isotope fractionation during the precipitation of calcium carbonate. *Earth Planet. Sci. Lett.* **1970**, *8*, 363–371. [CrossRef]
82. Grossman, E. Carbon isotopic fractionation in live benthic foraminifera—Comparison with inorganic precipitate studies. *Geochim. Cosmochim. Acta* **1984**, *48*, 1505–1512. [CrossRef]
83. Mees, F.; Reyes, E.; Keppens, E. Stable isotope chemistry of gaylussite and nahcolite from the deposits of the Crater Lake at Malha, northern Sudan. *Chem. Geol.* **1998**, *146*, 87–98. [CrossRef]
84. Turner, J.V. Kinetic fractionation of carbon-13 during calcium carbonate precipitation. *Geochim. Cosmochim. Acta* **1982**, *46*, 1183–1191. [CrossRef]
85. Sugiura, Y.; Onuma, K.; Yamazaki, A. Growth dynamics of vaterite in relation to the physico-chemical properties of its precursor, amorphous calcium carbonate, in the Ca-CO_3-PO_4 system. *Am. Miner.* **2016**, *101*, 289–296. [CrossRef]

86. Fernández-Díaz, L.; Fernández-González, A.; Prieto, M. The role of sulfate groups in controlling $CaCO_3$ polymorphism. *Geochim. Cosmochim. Acta* **2010**, *74*, 6064–6076. [CrossRef]
87. Clark, I.D.; Lauri, B. Kinetic enrichment of stable isotopes in cryogenic calcites. *Chem. Geol.* **1992**, *102*, 217–228.
88. Grasby, S.E. Naturally precipitating vaterite (μ-$CaCO_3$) spheres: Unusual carbonates formed in an extreme environment. *Geochim. Cosmochim. Acta* **2003**, *67*, 1659–1666. [CrossRef]
89. Kodina, L.A.; Tokarev, V.G.; Vlasova, L.N.; Korobeinik, G.S. Contribution of biogenic methane to ikaite formation in the Kara Sea: Evidence from the stable carbon isotope geochemistry. *Proc. Mar. Sci.* **2003**, *6*, 349–374.
90. Weiss, R.; Östlund, H.; Craig, H. Geochemical studies of the Weddell sea. *Deep Sea Res. Part A. Oceanogr. Res. Pap.* **1979**, *26*, 1093–1120. [CrossRef]
91. Lacelle, D.; Lauriol, B.; Clark, I.D. Formation of seasonal ice bodies and associated cryogenic carbonates in Caverne de I'Ours, Que bec, Canada: Kinetic isotope effects and pseudo-biogenic crystal structures. *J. Cave Karst Stud.* **2009**, *71*, 49–62.
92. Grossman, E.L. Applying oxygen isotope paleothermometry in deep time. *Paléontol. Soc. Pap.* **2012**, *18*, 39–68. [CrossRef]
93. O'Neil, J.R.; Clayton, R.N.; Mayeda, T.K. Oxygen isotope fractionation in divalent metal carbonates. *J. Chem. Phys.* **1969**, *51*, 5547–5558. [CrossRef]
94. Hays, P.; Grossman, E. Oxygen isotopes in meteoric calcite cements as indicators of continental paleoclimate. *Geology* **1991**, *19*, 441–444. [CrossRef]
95. Rickaby, R.; Shaw, S.; Bennitt, G.; Kennedy, H.; Zabel, M.; Lennie, A. Potential of ikaite to record the evolution of oceanic $\delta^{18}O$. *Geology* **2006**, *34*, 497–500. [CrossRef]
96. Bots, P.; Benning, L.G.; Rodriguez-Blanco, J.-D.; Roncal-Herrero, T.; Shaw, S. Mechanistic insights into the crystallization of amorphous calcium carbonate (ACC). *Cryst. Growth Des.* **2012**, *12*, 3806–3814. [CrossRef]
97. Tarutani, T.; Clayton, R.N.; Mayeda, T.K. The effect of polymorphism and magnesium substitution on oxygen isotope fractionation between calcium carbonate and water. *Geochim. Cosmochim. Acta* **1969**, *33*, 987–996. [CrossRef]
98. Kim, S.-T.; O'Neil, J.R. Equilibrium and nonequilibrium oxygen isotope effects in synthetic carbonates. *Geochim. Cosmochim. Acta* **1997**, *61*, 3461–3475. [CrossRef]
99. Kluge, T.; John, C.M. A simple method for vaterite precipitation in isotopic equilibrium: Implications for bulk and clumped isotope analysis. *Biogeosci. Discuss.* **2014**, *11*, 3289–3299.
100. Stewart, M.K. Hydrogen and oxygen fractionation during crystallization of mirabellite and ice. *Geochim. Cosmochim. Acta* **1974**, *38*, 167–172. [CrossRef]
101. Horita, J. Stable isotope fractionation factors of water in hydrated saline mineral-brine systems. *ESPL* **1989**, *95*, 173–179. [CrossRef]
102. Gonfiantini, R.; Fontes, J.R. Oxygen isotopic fractionation in the water of crystallization of gypsum. *Nature* **1963**, *200*, 644–646. [CrossRef]
103. Barrer, R.M.; Denney, E. Water in hydrates I.—Fractionation of hydrogen isotopes by crystallization of salt hydrates. *J. Chem. Soc.* **1964**, *904*, 4677–4684. [CrossRef]
104. Fontes, J.C.; Gonfiantini, R. Fractionnement isotopique de l'hydrogene dans l'esu de crystallisation du gypse. *C.R. Acad. Sci. Ser. D* **1967**, *265*, 4–6.
105. Kemper, E. Das Klima der Kreidezeit. *Geol. Jahrbuch A* **1987**, *96*, 5–185.
106. Huggett, J.M.; Schultz, B.P.; Shearman, D.J.; Smith, A.J. The petrology of ikaite pseudomorphs and their diagenesis. *Proc. Geol. Assoc.* **2005**, *116*, 3–4, 207–220. [CrossRef]
107. Selleck, B.W.; Carr, P.F.; Jones, B.G. A review and synthesis of glendonites (pseudomorphs after ikaite) with new data: Assessing applicability as recorders of ancient coldwater conditions. *J. Sediment. Res.* **2007**, *77*, 980–991. [CrossRef]
108. Schultz, B.; Thibault, N.; Huggett, J. The minerals ikaite and its pseudomorph glendonite: Historical perspective and legacies of Douglas Shearman and Alec K. Smith. *Proc. Geol. Assoc.* **2022**, *133*, 176–192. [CrossRef]
109. Butschli, O. Untersuchungen über organische Kalkgebilde, nebst Bemerkungen über organische Kieselgebilde, insbesondere über das spezifische Gewicht in Beziehung zu der Struktur, der chemischen Zusammensetzung und anderes. *Göttingen. Ges. D. Wiss. Abhandl.* **1908**, *6*, 1–177.
110. Mckenzie, J.E. Calcium carbonate hexahydrate. *J. Chem. Soc. Trans.* **1923**, *123*, 2409–2417. [CrossRef]
111. Kohlschutter, V.; Egg, C. Über Anderungen des Habitus und der Modifikation von Calcium-carbonat durch Lösungsgenossen. *Helv. Chim. Acta* **1925**, *8*, 479–484. [CrossRef]
112. Purgstaller, B.; Dietzel, M.; Baldermann, A.; Mavromatis, V. Control of temperature and aqueous Mg^{2+}/Ca^{2+} ratio on the trans formation of ikaite. *Geochim. Cosmochim. Acta* **2017**, *217*, 128–143. [CrossRef]
113. Clarkson, J.R.; Price, T.J.; Adams, C.J. Role of metastable phases in the spontaneous precipitation of calcium carbonate. *J. Chem. Soc. Faraday Trans.* **1992**, *88*, 243–249. [CrossRef]
114. Stockmann, G.; Tollefsen, E.; Skelton, A.; Brüchert, V.; Balic-Zunic, T.; Langhof, J.; Skogby, H.; Karlsson, A. Control of a calcite inhibitor (phosphate) and temperature on ikaite precipitation in Ikka Fjord, southwest Greenland. *Appl. Geochem.* **2018**, *89*, 11–22. [CrossRef]
115. Council, T.C.; Bennett, P.C. Geochemistry of ikaite formation at Mono Lake, California: Implications for the origin of tufa mounds. *Geology* **1993**, *21*, 971–974. [CrossRef]
116. Hu, Y.-B.; Wolthers, M.; Wolf-Gladrow, D.A.; Nehrke, G. Effect of pH and phosphate on calcium carbonate polymorphs precipitated at near-freezing temperature. *Cryst. Growth Des.* **2015**, *15*, 1596–1601. [CrossRef]

117. Zhou, X.; Lu, Z.; Rickaby, R.E.M.; Domack, E.W.; Wellner, J.S.; Kennedy, H.A. Ikaite abundance controlled by porewater phosphorus level: Potential links to dust and productivity. *J. Geol.* **2015**, *123*, 269–281. [CrossRef]
118. Ito, T. Factors controlling the transformation of natural ikaite from Shiowakka, Japan. *Geochem. J.* **1998**, *32*, 267–273. [CrossRef]
119. Hansen, M.O.; Buchardt, B.; Kühl, M.; Elberling, B. The fate of the submarine ikaite tufa columns in southwest greenland under changing climate conditions. *J. Sediment. Res.* **2011**, *81*, 553–561. [CrossRef]
120. Hu, Y.B.; Wolf-Gladrow, D.A.; Dieckmann, G.S.; Völker, C.; Nehrke, G. A laboratory study of ikaite ($CaCO_3 \cdot 6H_2O$) precipitation as a function of pH, salinity, temperature and phosphate concentration. *Mar. Chem.* **2014**, *162*, 10–18. [CrossRef]
121. Rodríguez-Ruiz, I.; Veesler, S.; Gómez-Morales, J.; Delgado-López, J.M.; Grauby, O.; Hammadi, Z.; Candoni, N.; García-Ruiz, J.M. Transient calcium carbonate hexahydrate (ikaite) nucleated and stabilized in confined nano- and picovolumes. *Cryst. Growth Des.* **2014**, *14*, 792–802. [CrossRef]
122. Berner, R.A.; Morse, J.W. Dissolution kinetics of calcium carbonate in seawater. IV. Theory of calcite dissolution. *Am. J. Sci.* **1974**, *274*, 108–134. [CrossRef]
123. Reddy, M.M. Crystallization of calcium carbonate in the presence of trace concentrations of phosphorus-containing anions. *J. Cryst. Growth* **1977**, *41*, 287–295. [CrossRef]
124. Froelich, P.; Klinkhammer, G.; Bender, M.; Luedtke, N.; Heath, G.; Cullen, D.; Dauphin, P.; Hammond, D.; Hartman, B.; Maynard, V. Early oxidation of organic matter in pelagic sediments of the eastern equatorial Atlantic: Suboxic diagenesis. *Geochim. Cosmochim. Acta* **1979**, *43*, 1075–1090. [CrossRef]
125. Burton, E.A.; Walter, L.M. The role of pH in phosphate inhibition of calcite and aragonite precipitation rates in seawater. *Geochim. Cosmochim. Acta* **1990**, *54*, 797–808. [CrossRef]
126. Lin, Y.-P.; Singer, P.C. Inhibition of calcite precipitation by orthophosphate: Speciation and thermodynamic considerations. *Geochim. Cosmochim. Acta* **2006**, *70*, 2530–2539. [CrossRef]
127. Mucci, A. Growth kinetics and composition of magnesian calcite overgrowths precipitated from seawater: Quantitative influence of orthophosphate ions. *Geochim. Cosmochim. Acta* **1986**, *50*, 2255–2265. [CrossRef]
128. Lebrato, M.; Garbe-Schönberg, D.; Müller, M.N.; Blanco-Ameijeiras, S.; Feely, R.A.; Lorenzoni, L.; Molinero, J.-C.; Bremer, K.; Jones, D.O.B.; Iglesias-Rodriguez, D.; et al. Global variability in seawater Mg:Ca and Sr:Ca ratios in the modern ocean. *Proc. Natl. Acad. Sci. USA* **2020**, *117*, 22281–22292. [CrossRef]
129. Vickers, M.L.; Vickers, M.; Rickaby, R.E.; Wu, H.; Bernasconi, S.M.; Ullmann, C.V.; Bohrmann, G.; Spielhagen, R.F.; Kassens, H.; Schultz, B.P.; et al. The ikaite to calcite transformation: Implications for palaeoclimate studies. *Geochim. Cosmochim. Acta* **2022**, *334*, 201–216. [CrossRef]
130. Broecker, W.; Yu, J. What do we know about the evolution of Mg to Ca ratios in seawater? *Paleoceanography* **2011**, *26*. [CrossRef]
131. Vasileva, K.; Zaretskaya, N.; Ershova, V.; Rogov, M.; Stockli, L.D.; Stockli, D.; Khaitov, V.; Maximov, F.; Chernyshova, I.; Soloshenko, N. New model for seasonal ikaite precipitation: Evidence from White Sea glendonites. *Mar. Geol.* **2022**, *449*. [CrossRef]
132. Mitterer, R.M.; Cunningham, R. The interaction of natural organic matter with grain surfaces: Implications for calcium carbonate precipitation. In *Carbonate Cements*; Society for Sedimentary Geology: Tulsa, OK, USA, 1985; pp. 17–31. [CrossRef]
133. Braissant, O.; Cailleau, G.; Dupraz, C.; Verrecchia, E.P. Bacterially induced mineralization of calcium carbonate in terrestrial environments: The role of exopolysaccharides and amino acids. *J. Sediment. Res.* **2003**, *73*, 485–490. [CrossRef]
134. Stougaard, P.; Jørgensen, F.; Johnsen, M.G.; Hansen, O.C. Microbial diversity in ikaite tufa columns: An alkaline, cold ecological niche in Greenland. *Environ. Microbiol.* **2002**, *4*, 487–493. [CrossRef] [PubMed]
135. Schmidt, M.; Priemé, A.; Stougaard, P. Bacterial diversity in permanently cold and alkaline ikaite columns from Greenland. *Extremophiles* **2006**, *10*, 551–562. [CrossRef] [PubMed]
136. Vester, J.K.; Glaring, M.A.; Stougaard, P. Discovery of novel enzymes with industrial potential from a cold and alkaline environment by a combination of functional metagenomics and culturing. *Microb. Cell Factories* **2014**, *13*, 72. [CrossRef] [PubMed]
137. Rogov, M.A.; Ershova, V.B.; Shchepetova, E.V.; Zakharov, V.A.; Pokrovsky, B.G.; Khudoley, A.K. Earliest Cretaceous (late Berriasian) glendonites from Northeast Siberia revise the timing of initiation of transient Early Cretaceous cooling in the high latitudes. *Cretac. Res.* **2017**, *71*, 102–112. [CrossRef]
138. Rogov, M.; Ershova, V.; Vereshchagin, O.; Vasileva, K.; Mikhailova, K.; Krylov, A. Database of global glendonite and ikaite records throughout the Phanerozoic. *Earth Syst. Sci. Data* **2021**, *13*, 343–356. [CrossRef]
139. Morales, C.; Rogov, M.; Wierzbowski, H.; Ershova, V.; Suan, G.; Adatte, T.; Föllmi, K.B.; Tegelaar, E.; Reichart, G.-J.; De Lange, G.; et al. Glendonites track methane seepage in Mesozoic polar seas. *Geology* **2017**, *45*, 503–506. [CrossRef]
140. Watkins, J.M.; Nielsen, L.C.; Ryerson, F.J.; DePaolo, D.J. The influence of kinetics on the oxygen isotope composition of calcium carbonate. *Earth Planet. Sci. Lett.* **2013**, *375*, 349–360. [CrossRef]
141. Yumol, L.M.; Uchikawa, J.; Zeebe, R.E. Kinetic isotope effects during CO_2 hydration: Experimental results for carbon and oxygen fractionation. *Geochim. Cosmochim. Acta* **2020**, *279*, 189–203. [CrossRef]
142. Sade, Z.; Halevy, I. New constraints on kinetic isotope effects during CO_2(aq) hydration and hydroxylation: Revisiting theoretical and experimental data. *Geochim. Cosmochim. Acta* **2017**, *214*, 246–265. [CrossRef]
143. Galimov, E.M.; Kodina, L.A.; Stepanets, O.V.; Korobeinik, G.S. Biogeochemistry of the Russian Arctic. Kara Sea: Research results under the SIRRO project, 1995–2003. *Geochem. Int.* **2006**, *44*, 1053–1104. [CrossRef]
144. Hiruta, A.; Matsumoto, R. Geochemical comparison of ikaite and methane-derived authigenic carbonates recovered from Echigo Bank in the Sea of Japan. *Mar. Geol.* **2021**, *443*, 106672. [CrossRef]

145. Brandt, K. Glacioeustatic cycles in the Early Jurassic? *Neues Jahrb. Geolog. Paläontol. Mon.* **1986**, *6*, 257–274. [CrossRef]
146. Frakes, L.A.; Francis, J.E. A guide to Phanerozoic cold polar climates from high-latitude ice-rafting in the Cretaceous. *Nature* **1988**, *333*, 547–549. [CrossRef]
147. Sheard, M.J. Glendonites from the southern Eromanga Basin in South Australia: Palaeoclimatic indicators for Cretaceous ice. *Geol. Surv. S. Australia, Quart. Geol. Notes* **1990**, *114*, 17–23.
148. Brandley, R.T.; Krause, F.F. Thinolite-type pseudomorphs after ikaite: Indicators of cold water on the subequatorial western margin of Lower Carboniferous North America. *Can. Soc. Petrol. Geolog. Memoir* **1994**, *17*, 333–344.
149. Parrish, J.T.; Bradshaw, M.T.; Brakel, A.T.; Mulholland, S.M.; Totterdell, J.M.; Yeates, A.N. Palaeoclimatology of Australia during the Pangean interval. *Palaeoclimates* **1996**, *1*, 241–281.
150. Johnston, J.D. Pseudomorphs after ikaite in a glaciomarine sequence in the Dalradian of Donegal, Ireland. *Scott. J. Geol.* **1995**, *31*, 3–9. [CrossRef]
151. Yan, J. Ikaite pseudomorphs, cold water indicators in the Chihsia Formation (Early Permian) of South China (abstract): 30th Intern. *Geol. Congr.* **1996**, *30*, 97.
152. De Lurio, J.L.; Frakes, L.A. Glendonites as a paleoenvironmental tool: Implications for early Cretaceous high latitude climates in Australia. *Geochim. Cosmochim. Acta* **1999**, *63*, 1039–1048. [CrossRef]
153. Shi, G.R. Possible influence of Gondwanan glaciation on low-latitude carbonate sedimentation and trans-equatorial faunal migration: The Lower Permian of South China. *Geosci. J.* **2001**, *5*, 57–63. [CrossRef]
154. Swainson, I.P.; Hammond, R.P. Hydrogen bonding in ikaite, $CaCO_3 \cdot 6H_2O$. *Miner. Mag.* **2003**, *67*, 555–562. [CrossRef]
155. Buchardt, B.; Israelson, C.; Seaman, P.; Stockmann, G. Ikaite tufa towers in Ikka Fjord, southwest Greenland: Their formation by mixing of seawater and alkaline spring water. *J. Sed. Res.* **2001**, *71*, 176–189. [CrossRef]